Recent progress on exploring mu-oxo bridged binuclear porphyrinoid complexes in catalysis and material science

A. Sorokin

Recent progress on exploring μ-oxo bridged binuclear porphyrinoid complexes in catalysis and material science

Alexander B. Sorokin

Institut de Recherches sur la Catalyse et l'Environnement de Lyon, IRCELYON, UMR 5256, CNRS – Université Lyon 1, 2, avenue Albert Einstein, 69626 Villeurbanne Cedex, France
e-mail : alexander.sorokin@ircelyon.univ-lyon1.fr

Dedicated to Professor Armando J.L. Pombeiro for his outstanding achievements in Coordination Chemistry and Catalysis

Abstract

This review covers recent advances in the preparation, characterization and application of μ-oxo dimeric complexes with different metals and non-metal and macrocyclic ligands achieved during last ten years. Binuclear iron, manganese, ruthenium, chromium, molybdenum, rhenium, aluminium, silicon, phosphorus and boron oxygen-bridged complexes supported by phthalocyanine, porphyrin, porphyrazine, corrole, tetrabenzotriazacorrole, subphthalocyanine and subporphyrin ligands have been prepared and characterized demonstrating a great versatility of μ-oxo binuclear macrocyclic platform which can accommodate a myriad of homoleptic and heteroleptic combinations with the same or different metal sites. They exhibit interesting structural and electronic properties allowing their increasing use in catalysis, optoelectronic, medical and other applications.

Keywords

μ-oxo dimer; phthalocyanine; porphyrin; binuclear; catalysis

1. Introduction

Metal sites of phthalocyanine, porphyrin and related macrocycles can be connected by μ-oxo, μ-nitrido and μ-carbido bridges to form an interesting class of binuclear single-atom bridged macrocyclic complexes. The synthesis, characterization, properties and applications of these complexes have been reviewed [1-3]. While mononuclear porphyrin [4], phthalocyanine [5,6], corrole [7] and porphyrazine [8] complexes have been widely recognized as catalysts for a variety of reactions, their single-atom bridged binuclear counterparts have been considered as catalytically inert for a long time. Only in 1999 we have found that supported μ-oxo diiron phthalocyanines efficiently catalyzed the oxidation of aromatic compounds to quinones [9]. Moreover, their catalytic properties are often superior than those of their mononuclear counterparts [10]. Significantly, a dimeric structure of μ-oxo diiron complexes plays an essential role in their catalytic activity in oxidation reactions [11-14]. When the active oxidizing species is formed, the oxidation state of iron site(s) is increased by two redox equivalents (Fig. 1).

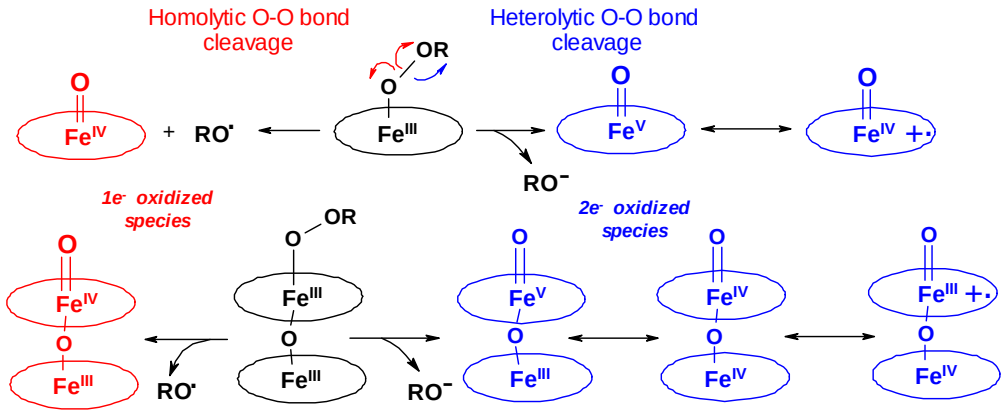

Fig. 1. Formation of active oxo species starting from iron monomeric and dimeric μ-oxo porphyrin-like complexes. Oval stands for macrocyclic ligand.

Binuclear construction should better stabilize this high oxidation state via delocalization of the charge at two iron sites and two macrocyclic ligands than mononuclear complex with one iron site and one macrocyclic ligand. Hence, heterolytic cleavage of O-O bond of peroxo complex to generate Compound I - like oxo species should be more favorable in the case binuclear platforms. In addition, mono- and binuclear oxo species can exhibit different reactivity. For this reason, binuclear single-atom bridged complexes can be

considered as promising oxidation catalysts. Later, Nemykin and co-workers confirmed the catalytic activity of μ-oxo complexes in homogeneous oxidation of arenes and alkylaromatic compounds using hypervalent iodine oxidants [15,16]. In turn, binuclear non-heme iron, manganese and copper complexes connected by μ-oxo bridges have been widely used as catalysts for C-H bonds oxidative functionalization [17].

The interest to single-atom bridged porphyrinoid complexes has been renewed after discovery of the remarkable catalytic properties of μ-nitrido diiron phthalocyanines [18-25]. The rich catalytic chemistry of these complexes has been recently reviewed [26,27]. Recent studies suggest that μ-carbido diiron complexes can be also used as catalysts for oxidation [28-30]. μ-Carbido ruthenium phthalocyanine was shown to be efficient in the cyclopropanation of olefins and carbene insertion into the N-H bonds of amines [31].

Significant progress has been also achieved in μ-oxo dimeric porphyrinoid complexes since their chemistry has been reviewed [1,3,32]. This review highlights recent advances in synthesis and investigation of μ-oxo binuclear porphyrinoid complexes achieved during last ten years. This flexible platform provides an unique possibility to combine very different macrocyclic ligands in homoleptic or heteroleptic arrangements which involve different metals and non-metals to form homo- and heterometallic complexes (Fig. 2).

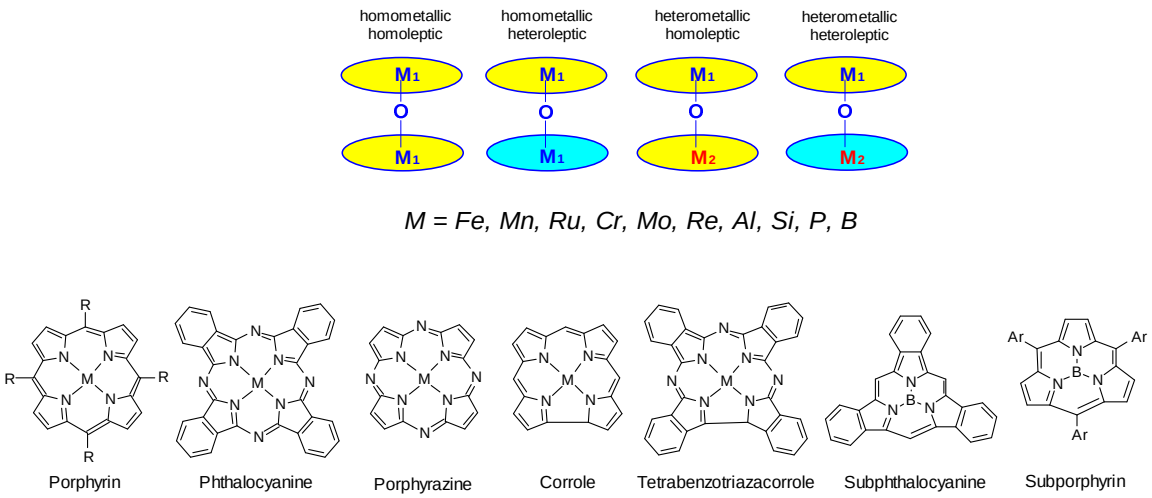

Fig. 2. General structures of homo- and heterometallic complexes in homo- and heteroleptic ligand environment. μ-Oxo dimers of different elements supported by macrocyclic ligands described in this review.

Extensive studies from many groups demonstrate the great utility of these versatile complexes in very different areas, starting from catalysis to optoelectronic applications.

2. μ-Oxo binuclear complexes

Two macrocyclic complexes involving different metals as well as silicon, phosphorus and boron (contracted porphyrinoids) and different macrocycles are connected by μ-oxo bridging group. The formed dimeric structure can be supported either by non-covalent interactions or through covalent linkage of two porphyrinoids by linkers of different length and flexibility to improve the stability of μ-oxo construction or/and to provide a desirable conformation. The structural and physical properties of μ-oxo macrocyclic complexes according to macrocyclic ligand and metalic or non-metallic centre are described below.

2.1. Phthalocyanines

2.1.1. Iron

Early works reported the preparation of two forms of μ-oxo diiron phthalocyanines having different X-ray powder patterns, IR, Mössbauer spectral properties and magnetic behaviour [1]. Both unsubstituted and substituted phthalocyanine ligands can be used to access to these unexpected isomeric complexes. The first μ-oxo dimer, μ-oxo(1), was prepared from FePc in organic solvents (DMF, DMA, THF, dioxane, DMSO). The second μ-oxo dimer, μ-oxo(2), was obtained using 96% H_2SO_4, 1-chloronaphthalene or in the presence of 2-propaneamine. μ-Oxo(2) can also be prepared by dissolving μ-oxo(1) in 96% H_2SO_4 followed by reprecipitation in cold water. Both μ-oxo complexes showed high thermal stability, very similar reflectance spectra and identical UV-vis spectra in 96% H_2SO_4 or in pyridine. The preparation and properties of these compounds have been discussed in details in the excellent review by Ercolani and co-workers [1]. Three structures of the μ-oxo diiron species were suggested which adopted either different geometrical organization with parallel or bent phthalocyanine planes or different oxidation state (Fe^{III}-O-Fe^{III} or Fe^{II}-O-Fe^{II}) [33-36]. This point was a subject of a long discussion and finally, on the basis of solid experimental data, two structures have been assigned as phthalocyanine dimers with bent and linear Fe^{III}-O-Fe^{III} fragments for μ-oxo(1) and μ-oxo(2), respectively, which exhibit quite different IR spectra, magnetic moments, antiferoomagnetic coupling and Mössbauer parameters (Fig. 3).

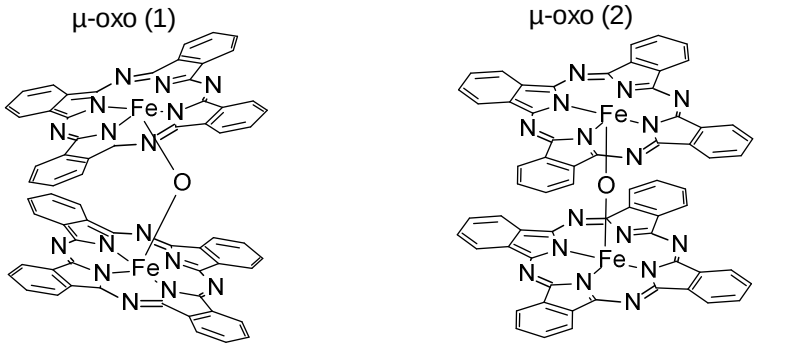

ν_{as} (Fe-O-Fe) = 824, 852 cm^{-1}
μ_B = 2.09 – 2.22 per Fe atom
J = -120 cm^{-1}
δ = 0.37 mm s^{-1}, ΔE_Q = 0.44 mm s^{-1}

ν_{as} (Fe-O-Fe) - absent
μ_B = 1.39 – 1.47 per Fe atom
J = -195 cm^{-1}
δ = 0.26 mm s^{-1}, ΔE_Q = 1.26 mm s^{-1}

Fig. 3. Schematic representation of two μ-oxo diiron complexes with unsubstituted phthalocyanine ligands and their principal properties.

To provide structural flexibility, elaborated supramolecular heteroleptic μ-oxo diiron complex with porphyrin and phthalocyanine ligands linked by a highly flexible fourfold rotaxane was prepared by Tanaka and co-workers (Fig. 4) [37].

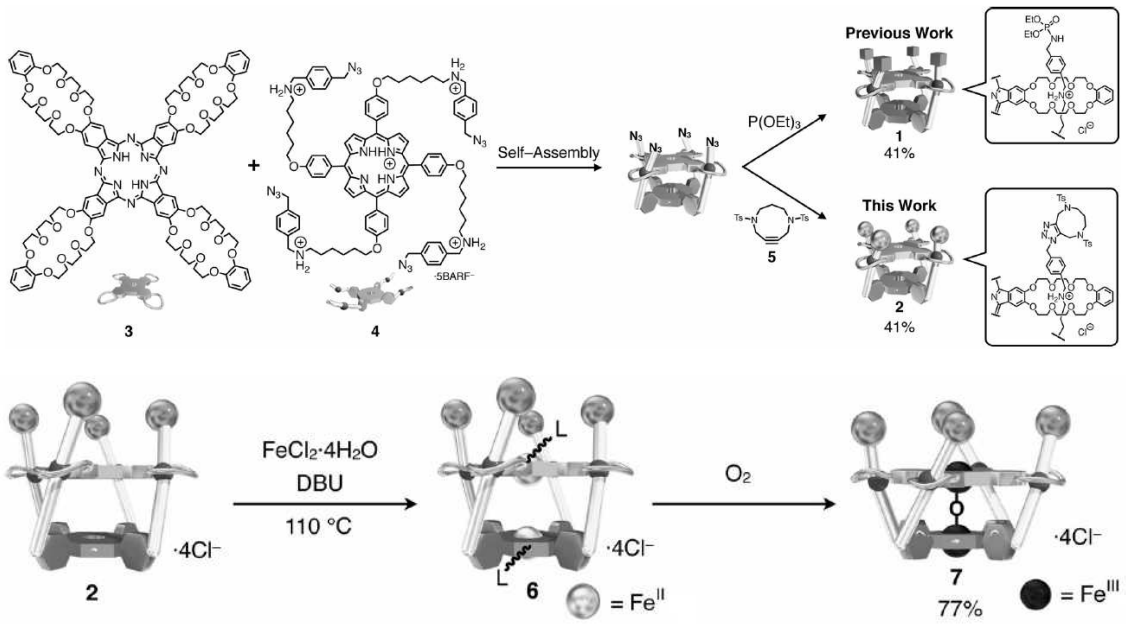

Fig. 4. Preparation of a fourfold rotaxane μ-oxo heteroleptic dimer with phthalocyanine and porphyrin macrocycles. Reprinted with permission from ref. [37]. Copyright 2017 Wiley and Sons.

In the first step, conjugates **1** and **2** between non-metalated phthalocyanine and porphyrin units were self-assembled due to the non-covalent interaction between crown moieties of phthalocyanine and positively charged ammonium groups of porphyrin. These structures were stabilized using phosphoramide or triazole stoppers. The conjugate **2** was metalated with $FeCl_2$ in the presence of DBU at 110°C to provide binuclear Fe(II) complex **6** which was converted to diamagnetic μ-oxo diiron(III) complex **7** by aerobic oxidation via the formation of μ-peroxo complex followed by its reduction with excess $FeCl_2$. The FEFF fitting analysis of the Fe K-edge extended X-ray absorption fine structure (EXAFS) data provided Fe-O and Fe-Fe distances of 1.81 and 3.47 Å, respectively. These longer distances with respect to regular μ-oxo dimeric complexes indicate structural adaptability of this scaffold which can be useful for electrochemical catalytic oxygen reduction [37]. Prepared by the same group related CuPor-CuPc [38] and CuPor-ZnPc [39] assemblies were just cofacially stacked with no μ-oxo bridge resulting in a longer metal-metal distance of 7 Å which indicates significant structural adaptability of this construction.

μ-Oxo dimer of iron phthalocyanine bearing 5-oxy-dimethylisophthalate groups in non-peripheral positions was synthetized in 16.7 % yield [40]. Successful preparation of μ-oxo dimer despite significant sterical demand exerted by bulky substituents also indicates the flexibility of the μ-oxo construction. Spectroelectrochemical study indicated a decomposition of the complex during the electrolysis at 0.75 V (SCE) suggesting the formation of oxidizing species under these conditions.

2.1.2. Chromium

Chromium phthalocyanine complexes exhibit multiple metal and ring oxidation states [41]. Treatment of $Cr^{II}Pc$ with 0.5 equiv of PhIO or air generated $(Cr^{III}Pc)_2O$ with axially coordinated THF molecules. The two Pc ligands are slightly distorted from planarity accommodating a nearly linear Cr-O-Cr fragment (177.6° angle) with Cr-O distances of 1.749 and 1.752 Å comparable with M-O distances in Fe and Mn counterparts [41]. The cyclic voltammogram of $(Cr^{III}Pc)_2O$ displays two reversible oxidation peaks at $E_{1/2}$ of 0.945 and 1.25 V (vs Ag/AgCl) tentatively assigned to stepwise oxidation of the Pc ligands. The CV showed several irreversible waves in the reduction part due to decomposition of $(Cr^{III}Pc)_2O$. The complex was also moisture-sensitive and generated $PcCr^{III}OH$ upon exposition of its THF solution to air. Attempts to chemically oxidize $(Cr^{III}Pc)_2O$ with $AgSbF_6$ in THF led to polymerization of THF suggesting that its oxidized form might exhibit some oxidizing properties.

2.1.3. Manganese

The $[MnPc(CN)]_2O$ complex was prepared by electrocrystallization technique in air [42]. A tetraphenylphosponium $[MnPc(CN)_2]$ solution in MeCN was subjected to a constant 1 μA current applied between two platinum electrodes for 2-3 weeks at 20°C. Platelike crystals were formed on the Pt anode. The twist angle between the Pc planes was determined to be 37° and the Mn-Mn distance was ~3.5 Å which is typical for Mn-O-Mn unit. However, X-ray analysis indicated structural disorder with non-equivalent Mn-O (1.761 and 1.747 Å for Mn_1-O and Mn_2-O, respectively) and Mn-CN distances (2.15 and 1.83 Å for Mn_1-CN and Mn_2-CN, respectively) originated from the stacking of the $[MnPc(CN)]_2O$ molecules in the crystal (Fig. 5) [42].

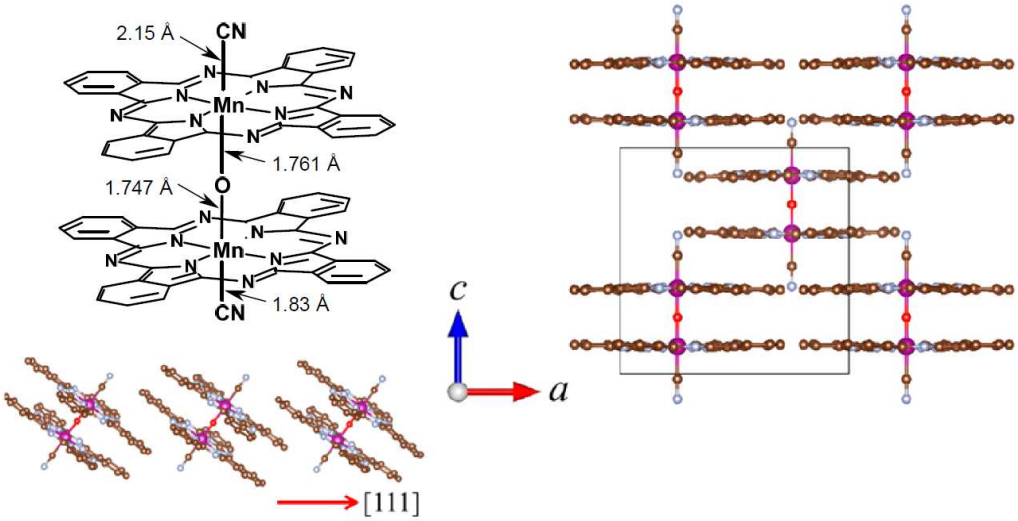

Fig. 5. Non-symmetrical molecular structure of $[MnPc(CN)]_2O$. Stacking of molecules along the [111] axis and view from the *b* axis. Adapted with permission from ref. [42]. Copyright 2016 American Chemical Society.

The IR spectrum of $[MnPc(CN)]_2O$ exhibited two bands of C≡N stretching vibrations at 2170 and 2186 cm^{-1} confirming the non-equivalence of Mn_1-CN and Mn_2-CN fragments. It was proposed that due to structural disorder the Mn_1 and Mn_2 atoms were in the different spin states ($S_{Mn1} = 0$ and $S_{Mn1} = 1$) thus explaining the effective magnetic moment of 3.16 μ_B.

μ-Oxo dimanganese phthalocyanine bearing thiazole substituents exhibited quite different redox behavior compared to mononuclear counterpart [43]. Due to the thiazole

groups this μ-oxo dimer was electropolymerized on the working electrode which catalyzed oxygen evolution reaction.

2.1.4. Aluminum

The use of phthalocyanine functionalized with crown ether units gives a possibility to change conformation of dimeric complex via non-covalent interactions of the crown moieties with cations. The formation of μ-oxo dimer of Al tetra-15-crown-5-phthalocyanine in the presence of polar organic solvents was investigated by UV-vis and ^{1}H NMR spectroscopy [44]. Interestingly, a μ-fluoro dimer of the Al crown-substituted phthalocyanine was also detected in the presence of the excess of Bu_4NF. Such bridged dimeric AlPc can be used as precursors for the organized polymeric materials that possess semiconducting and nonlinear optical properties. The alkali-metal-induced assembling of crown-Pc in solution can be used to access to dimeric structures [45]. Gorbunova and co-workers have recently published the first X-ray structure of such assembly. Cation-induced dimerization of crown-substituted phthalocyanine [(HO)Al(15C5)$_4$Pc] upon addition of an excess of potassium or rubidium nicotinate solutions in MeOH was evidenced by the blue shift of the Q band in the UV-vis spectra from 690 to 639 nm [46]. In the presence of ~10 equiv of RbNic the narrow high-field shifted singlet signal of aromatic protons at 8.83 ppm was observed. The α–CH_2 signal of the crown ether moieties split into two signals for exo and endo protons indicating the dimer formation. The structure of the supramolecular [(μ-oxo)bis(tetra-15-crown-5-phthalocyaninato)(nicotinato)-aluminum(III)]tetra(rubidium) bis(nicotinate) was determined by XRD using synchrotron radiation (Fig. 6) [46].

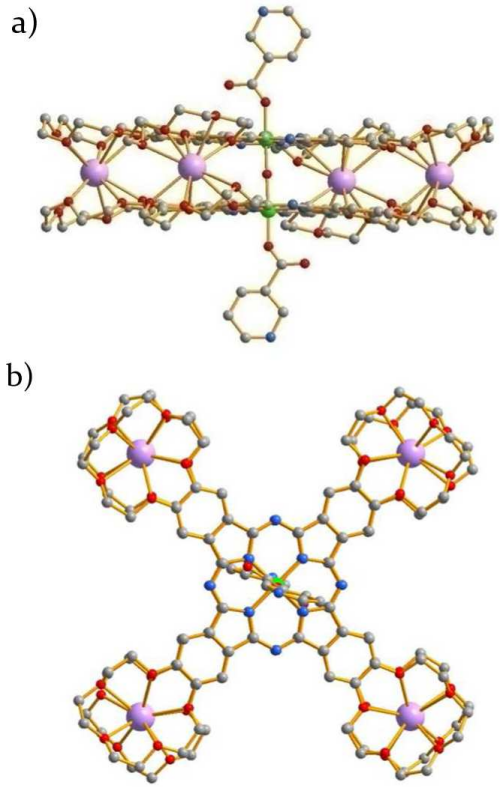

Fig. 6. X-ray structure of the [(μ-oxo)bis(tetra-15-crown-5-phthalocyaninato)(nicotinato)-aluminum(III)]tetra(rubidium) bis(nicotinate): a) side view; b) top view. Reprinted with permission from ref. [46]. Copyright 2018 American Chemical Society.

The Al-O length of the symmetrical linear Al-O-Al fragment is 1.881 Å. Interestingly, each Al center also bears axial nicotinate at 1.991 Å distance which leads to its almost in N_4 plane location with out-of-plane displacement only by 0.031 Å. This is in sharp contrast to published five-coordinated AlPc(L) and $(AlPc)_2O$ with the Al center 0.390-0.459 Å out of the phthalocyanine plane [47,48]. The longer Al-μO bond (1.881 Å) is another difference from reported five-coordinated $(PcAl)_2O$ (1.679 Å) [48] and $(PorphAl)_2O$ (1.675 Å) [49] structures with longer interplanar distances of 4.276 and 4.227 Å, respectively. Due to the accomodation of the large Rb^+ cations between crown ether moieties, the parallel phthalocyanine rings are exlipsed with an interplanar distance of 3.697 Å which is significantly shorter (~0.55 Å) than the corresponding distances in regular five-coordinated μ-oxo Al counterparts. Thus, such a short distance between aromatic phthalocyanine systems induced by additional bonding of four Rb^+ cations with crown ether moieties should favor π–π interaction and might result in particular properties of these interesting constructions. The structural parameters of regular μ-

oxo digallium(III) phthalocyanine and perfluorophthalocyanine complexes were determined by DFT calculations [50].

2.1.5. Silicon

μ-Oxo silicon-based phthalocyanine polymeric and oligomeric materials have been intensively studied because of their unique semiconductor behavior due to the cofacial π–conjugation of macrocycles with an interplanar distance of ~3.3 Å. In this context, the structures and the properties of μ-oxo silicon dimers continue to attract much attention to get deeper insight to the interaction between aromatic systems playing a crucial role in the conductivity of the polymers [51]. While μ-oxo homoleptic complexes have been comprehensively investigated, the importance of heteroleptic μ-oxo disilicon counterparts was only recently recognized and these compounds have began to attract considerable attention since recent synthetic developments. Thermal condensation of silicon phthalocyanine with peripheral butoxy groups and silicon naphthalocyanine (SiNc) in quinoline at 180°C furnished a heteroleptic μ-oxo dimer PcSi-O-SiNc with 20-25% yields [49]. The replacement of axial hydroxyl ligands with triphenylsilyloxy groups allowed to avoiding the severe aggregation of phthalocyanine cycles. Interestingly, the position of principal Q band at 682 nm is similar to that of mononuclear SiPc but no strong absorption was observed in the Q band region of SiNc (790 nm). This behavior is unusual because the absorption spectra of other heteroleptic μ-oxo species show a sum of the contributions from both monomeric macrocycles. Crystal structure of PcSi-O-SiNc showed an interplanar distance of 3.3 Å between the SiPc and SiNc moieties with the torsion angle of 18° between them. However, variable temperature ^{1}H NMR indicated C_{4v} symmetric conformation with torsion angles of 0 or 45° in $CDCl_3$ or a fast rotation within the NMR time scale and the presence of thermally equilibrated rotational isomers in toluene.

A versatile strategy to achieve multichromophore structures with complementary absorption properties based on the using of dihydroxysilicon 1,4,8,11,15,18,22,25-octakis(hexyl)phthalocyanine [SiPc(C_6H_{13})$_8$](OH)$_2$ was proposed by Cook and co-workers [52]. Unlike unsubstituted and 2,3,9,10,16,17,23,24-substituted counterparts, it does not form a stable μ-oxo dimer owing to sterically demanding alkyl chains. In contrast, it can react with unsubstituted dihydroxysilicon phthalocyanine PcSi(OH)$_2$ and dihydroxygermanium octaethylporphyrin GeOEP(OH)$_2$ to form heteroleptic μ-oxo dimers PcSi-O-SiPc(C_6H_{13})$_8$ and OEPGe-O-SiPc(C_6H_{13})$_8$, respectively. Using this approach, a variety of multichromophore arrays absorbing across the complete UV-visible region and into the near-IR have been

prepared [52]. The staggering angles between adjacent phthalocyanines in oxygen-bridged silicon phthalocyanine oligomers were not distributed randomly but they were organized in two clusters with 16° and 41° [53].

Dihydroxysilicon 1,4,8,11,15,18,22,25-octakis(hexyl)phthalocyanine reacted at one face to furnish Cl-Si(Pc)-O-(Pc)Si-Cl [54]. Similarly, dihydroxygermanium octaethylporphyrin was used to obtain a stable µ-oxo linked dimeric complex. Interestingly, heteroleptic dimer prepared from dihydroxysilicon 1,4,8,11,15,18,22,25-octakis(hexyl)phthalocyanine and dihydroxysilicon octaethylporphyrin was unstable and could not be isolated. This synthetic strategy was also applied to non-peripherally substituted dihydroxysilicon phthalocyanine and dihydroxygermanium octaethylporphyrin to construct µ-oxo heterodiads and triads in controlled manner (Fig. 7) [55].

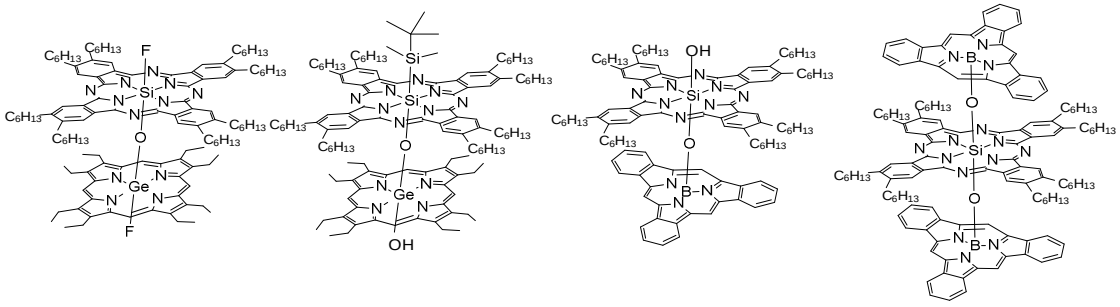

Fig. 7. Heteroleptic µ-oxo dimer and trimer structures prepared in [55] from silicon phthalocyanine and germanium octaethylporphyrin or boron subphthalocyanine.

Dihydroxysilicon phthalocyanine has also linked to chlorosubphthalocyanine to form Si-O-B dyad and triad [55]. µ-Oxo silicon tetrasubstituted phthalocyanines bearing SC_6H_{13} and $SC_{12}H_{25}$ groups exhibited decreased fluorescence quantum yield and lifetime values compared with the parent $(PcSi)_2O$ [56]. These µ-oxo species provided more efficient $^1O_2$ generation with respect to corresponding monomeric complexes.

2.2. Porphyrins

2.2.1. Iron

µ-Oxo diiron porphyrin complexes have been extensively investigated and early structural and spectroscopic data can be found in detailed review by Ercolani and coworkers [1]. Recent review from Rath group summarizes structurally characterized µ-oxo diiron complexes supported by porphyrin-like macrocycles (oxoporphyrin, azaporphyrin,

porphyrazine, corrole, porphodimethene, dioxoporphodimethene and chlorine) as well as linked and non-linked porphyrin units [57].

Binuclear arrangement brings about particular properties of μ-oxo dimeric complexes. Due to strong interaction of iron sites with the bridging oxygen atom, the Fe-O distances are generally shorter in μ-oxo dimers compared with iron - axial ligand distances in corresponding mononuclear complexes leading to more intense pre-edge peak of μ-oxo dimers $(FeTPP)_2O$ and $(FePPIX)_2O$ in Fe K-edge XANES spectra [58].

The (μ-oxo)bis[*meso*-tetrakis(*p*-bromophenylporphyrinato)iron(III)] complex was prepared under solvothermal conditions by incubation of a monomer solution in DMF at 120°C for 24 h [59]. Upon μ-oxo dimer formation, the Soret band was blue-shifted from 418 nm for the monomer to 408 nm for the dimer indicating π–π interaction between the two porphyrin planes. Two equivalent Fe-O bonds (1.761 Å) form Fe-O-Fe fragment with angle of 174.4° and iron atoms displaced out of the N_4 porphyrin plane by 0.494 Å. The Fe-O-Fe stretching vibration in the IR spectrum was observed at 881 cm^{-1}.

The (μ-oxo)bis[*meso*-tetrakis(*p*-carboxyphenylporphyrinato)iron(III)] complex was used for the synthesis of coordination networks of μ-oxo dimer molecules connected via carboxyl groups [60]. Two practically parallel porphyrin planes (angle between the planes = 0.31°) were found to be in staggered configuration with dihedral angle of 33.6°. The almost linear Fe-O-Fe fragment (179.78°) contains two equivalent Fe-O bonds of 1.7597 Å. This dimer forms a 2D layer structure due to hydrogen bonding of carboxyl groups and interaction between porphyrin planes of neighboring layers with the distance of 3.70 Å. (Fig. 8).

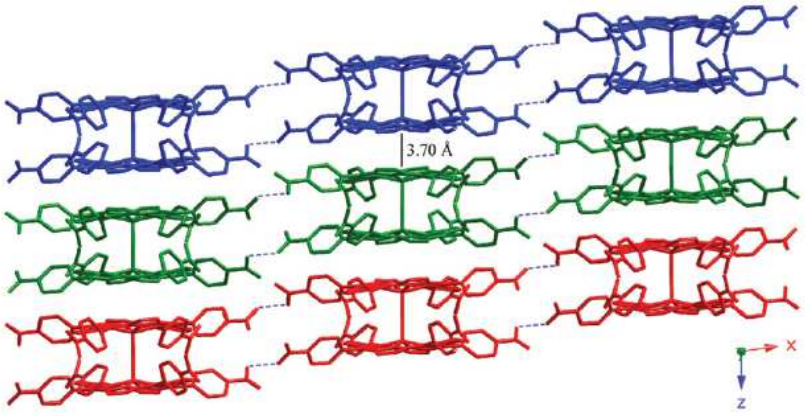

Fig. 8. Stacking 2D structure formed by (μ-oxo)bis[*meso*-tetrakis(*p*-carboxyphenylporphyrinato)iron(III)] complex. Reprinted with permission from ref. [60]. Copyright (2015) Royal Society of Chemistry.

The Mössbauer parameters (δ = 0.27 mm s^{-1} and ΔE_Q = 0.62 mm s^{-1}) as well as the temperature dependence of magnetic susceptibility of the dimer indicate a strong antiferromagnetic coupling of the high-spin Fe(III) sites with J = -132 cm^{-1}.

The (μ-oxo)bis[*meso*-tetrakis(pentafluorophenylporphyrinato)iron(III)] complex, $(FeTF_5PP)_2O$, was obtained after refluxing a mixture of free-base porphyrin with $FeCl_2$ in dry DMF in the presence of Py followed by incubation of the reaction mixture under air for 18 h [61]. An essentially linear Fe-O-Fe fragment (178.4°) is formed by the equivalent Fe-O bonds (1.773 Å). Electrospray mass-spectrometry is a convenient tool in the characterization of μ-oxo binuclear complexes given the right choice of the solvent [62]. Using of MeOH or CH_2Cl_2 allows detecting the strong molecular peak of μ-oxo species whereas the presence of acid additives results in their monomerization.

The X-ray structure of μ-oxo diiron octaethylporphyrin $(FeOEP)_2O$ with two parallel porphyrin rings (Fe-O-Fe angle = 180°) and typical Fe-O distances of 1.774 Å was determined by Saffari and co-workers [63]. This triclinic crystalline form differs from two crystalline forms published by Scheidt et al. [64]. While previous triclinic and monoclinic forms were in staggered conformations with twist angles of 17.0° and 16.8°, respectively, [64] this $(FeOEP)_2O$ crystals are in almost eclipsed configuration (twist angle = 1.2°) [63]. Balch and coworkers have prepared black crystals of $(FeOEP)_2O$ co-crystallized with fullerene and benzene [65]. While in the triclinic and monoclinic polyforms of $(FeOEP)_2O$ the Fe-O-Fe fragments are close to linear with the angles of 172.16° and 176.2°, respectively, in the $C_{60} \cdot (FeOEP)_2O \cdot C_6H_6$ hybrid material the Fe-O-Fe angles are remarkably bent (150.18° and 151.89°) due to rare incorporation of benzene molecule into the opening between the two porphyrin planes (Fig. 9).

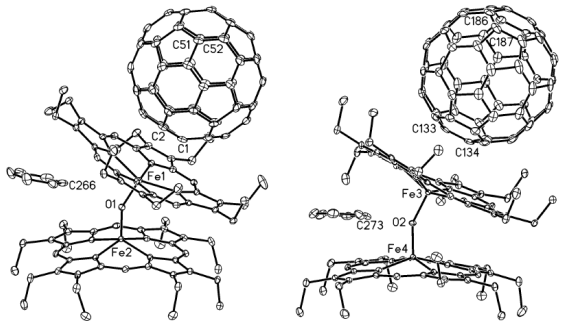

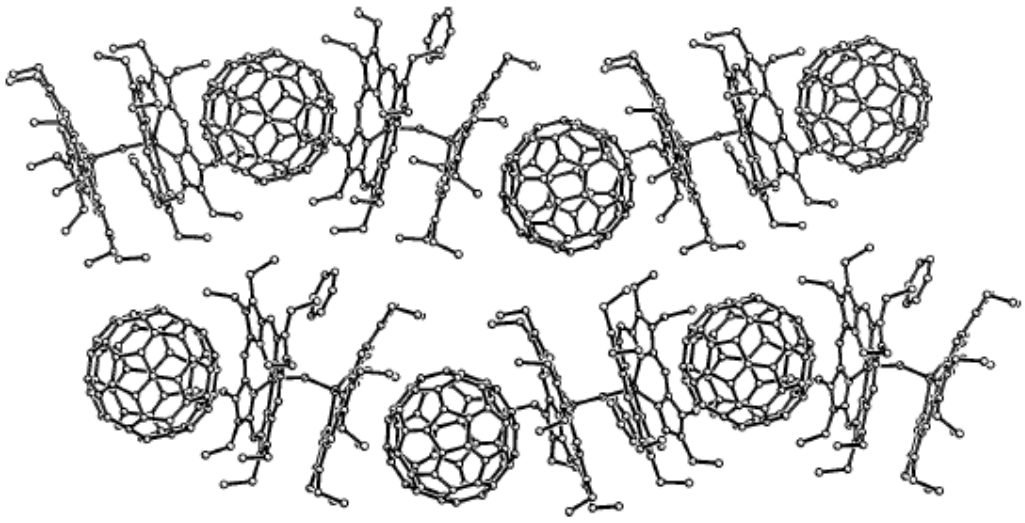

Fig. 9. Two distinct entities in the asymmetric unit of $C_{60} \cdot (FeOEP)_2O \cdot C_6H_6$ (a) and the molecular packing in the crystal structure of $C_{60} \cdot (FeOEP)_2O \cdot C_6H_6$ (b). Adapted with permission from Crystal Growth & Design 3 (2003) 691-697. Copyright (2003) American Chemical Society.

Interestingly, there is no π–π contact between the porphyrin system and the benzene molecule. In addition, no close contact between hydrogen atoms of C_6H_6 and the μ-oxo atom was observed.

μ-Oxo diiron complexes of 2,3,7,8,12,18-hexamethyl-13,17-dibutyl-5-monoazaporphine $(FeMAP)_2O$ and 3,7,13,17-hexamethyl-2,8,12,18-tetrabutyl-5,15-diazaporphine $(FeDAP)_2O$ were prepared and the X-ray structure of $(FeDAP)_2O$ was determined [66]. The Fe1 and Fe2 atoms were displaced from the mean N_4-coordinating plane by 0.572 and 0.565 Å with Fe1-O and Fe2-O distances of 1.777 and 1.776 Å, respectively. Non-coplanar arrangement of two macrocyclic ligands with tilt angle of 26.3° resulted in Fe1-O-Fe2 angle of 152.1° allowing for the close approach of wedged benzene molecule to μ-oxo atom at 2.584 Å distance (Fig. 10).

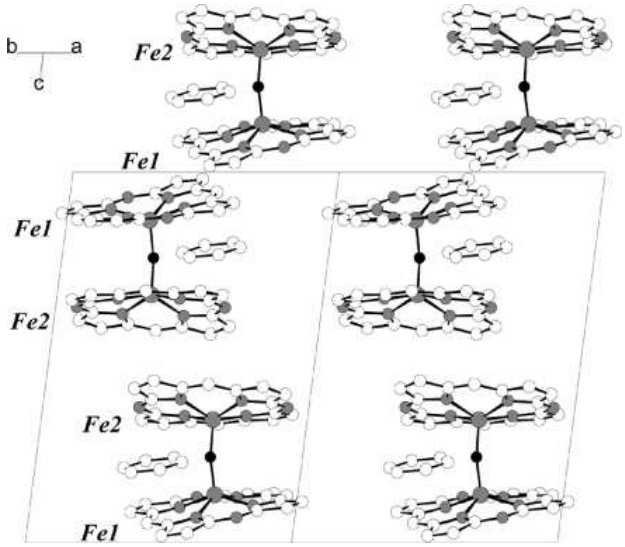

Fig. 10. Molecular packing of $(FeDAP)_2O \cdot (C6H6)$ View along [110] axis. Alkyl groups are omitted for clarity. Reprinted from ref. [66] with permission. Copyright (2011) John Wiley and Sons.

The detailed kinetic analysis showed that the stability of μ-oxo bridge in the presence of acids depended on its accessibility. The stability of dimer with flexible alkyl substituents in β–pyrrolic positions was notably lower than in the case of shielding *meso*- or β–phenyl groups.

Interestingly, several lines of evidence showed that chloroquine (CQ), archetypal antimalarial drug, induced the formation of μ-oxo dimer of Fe protoporphyrin IX, $(FePPIX)_2O$, which lacked the characteristic IR Fe-O-Fe vibration around 880 cm^{-1} [67]. The mechanism of the interaction of CQ with Fe(III)protoporphyrin IX has attracted a significant attention because CQ inhibits the hemozoin formation produced within malaria parasite in order to avoid intoxication. The interaction of $(FePPIX)_2O$ with CQ was probed using molecular dynamic simulations [68]. Two models of the $(FePPIX)_2O$ – CQ conjugate were studied: (i) π–stacked model with CQ placed at the external porphyrin face of $(FePPIX)_2O$ and (ii) docked model with CQ intercalated between the two porphyrin planes of $(FePPIX)_2O$. The feasibility of these models was investigated by fitting calculated model structures to the experimental EXAFS data obtained in frozen aqueous solution which were different from that of dried $(FePPIX)_2O$ solid [69]. The docked model with CQ intercalated inside of μ-oxo dimer cavity fitted better with experimental EXAFS spectrum. Noteworthy, the EXAFS fit showed a much longer Fe-O distance (1.87 Å) compared with typical Fe-O bond lengths in μ-

oxo dimers (1.76 ± 0.01 Å). For this reason, the asymmetric Fe-O-Fe stretching was detected at 744 cm^{-1} using ^{18}O isomer shift (to 704 cm^{-1}) instead of ~880 cm^{-1} typically observed in μ-oxo diiron complexes. Magnetic data also strongly support the presence of μ-oxo dimeric fragment with elongated Fe-O bond. The magnetic moment of 2.25 ± 0.02 μ_B determined for $(FePPIX)_2O$ – CQ at 30°C corresponded to an exchange coupling constant J = -86 ± 2 cm^{-1} which was notably weaker than that for typical μ-oxo diiron species, but still significantly stronger than that of μ-hydroxo diiron complexes [69].

2.2.2. Manganese

Coordination chemistry of porphyrin, phthalocyanine and related macrocycles at the solid/vacuum interface is a rapidly growing research area [70]. These flat structurally rigid molecules tend to strongly adsorb onto the surface in parallel fashion forming two-dimentional coordination network. Due to the influence of surface (the concept "surface trans effect") and the absence of solvent, the properties of adsorbed complexes significantly differ from those in homogeneous solutions. De Feyter and co-workers have published a prominent example of the preparation of μ-oxo dimer at the nanoscale [71]. Applying a pulse voltage with the STM tip (STM – scanning tunneling microscopy) to monolayer of TPPMnCl onto highly oriented pyrolytic graphite induced a local chemical reaction with O_2 resulting in the formation of $(TPPMn)_2O$ grafted at the graphite surface. It was proposed that initially formed $TPPMn^{III}$-O-$O^{\cdot}$ species looses oxygen atom to generate $TPPMn^{IV}$=O which is capable of reacting with another TPPMn molecule at the surface to produce $(TPPMn)_2O$.

2.2.3. Ruthenium

Ruthenium(IV) μ-oxo porphyrin complexes $[Ru^{IV}(TPP)(X)]_2O$ (X = OCH_3, *m*-chlorobenzoate) were prepared form $[Ru^{II}(TPP)(CO)(MeOH)$ and *m*-CPBA [72]. The ^1H NMR spectra showed typical pattern of a μ-oxo tetraphenylporphyrin complex with aromatic protons split into five signals. The $[Ru^{IV}(TPP)(OCH_3)]_2O$ complex reacted with azides RN_3 having good leaving group for electrophilic substitution (R = Ph_3C, Me_3Si) to generate a new μ-oxo complex $[Ru^{IV}(TPP)(N_3)]_2O$ characterized by X-ray diffraction analysis. Two slightly distorted porphyrin planes are almost parallel to each other and staggered by ~28° due to steric hindrance produced by phenyl substituents which tilted by 50-65° with respect to porphyrin planes. The Ru-O distances are 1.796 and 1.798 Å while each azide group has two main bent orientations with Ru-N-N angles of 126.7° and 121.2° and Ru-N length of 2.05 Å.

This study provides a rare example of the X-ray structure of μ-oxo dimer with two supplementary axial ligands [72].

2.2.4. Molybdenum, Rhenium

μ-Oxo dimeric complex of $TPPMo^{V}=O$ was obtained by passing the monomer solution through the basic Al_2O_3 column (CH_2Cl_2/ethyl acetate eluent) followed by the evaporation of solvents [73]. The terminal Mo=O bond length and the bridging Mo-O bond distances were 1.720 and 1.939 Å, respectively. The IR vibrations of the terminal Mo=O and bridging Mo-O fragments were observed at 904 and 566 cm^{-1}, respectively. However, the $[TPPMo^{V}=O]_2O$ complex is unstable in the solution easily forming a monomeric oxo-hydroxo molybdenum porphyrin complex. Similarly, $(O=Re^{V}TPP)_2O$ obtained with a 75 % yield exhibited the IR vibrations of the terminal Re=O and bridging Re-O-Re fragments at 961 and 723, 854 cm^{-1}, respectively [74]. No data on the reactivity of these unusual μ-oxo dimeric species bearing oxo groups are available though it would be interesting to explore the possibility of the transfer of oxygen atom to organic substrates.

2.3. Porphyrazines

2.3.1. Iron

In comparison with porphyrin and phthalocyanine μ-oxo complexes, their porphyrazine counterparts have been less investigated though several species with different substitution pattern have recently been published. μ-Oxo diiron complex supported by fluorinated porphyrazine ligands was prepared by heating bis(pentafluorophenyl)maleonitrile with $Fe(CO)_5$ in boiling 1-bromonaphthalene followed by the treatment with Bu_4NOH (Fig. 11) [75].

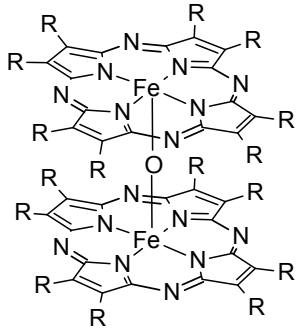

$[FePz(C_6F_5)_8]_2O$: R = C_6F_5
$[FePz(SC_2H_5)_8]_2O$: R = SC_2H_5
$[FePz(n\text{-}C_3H_7)_8]_2O$: R = $n\text{-}C_3H_7$

Fig. 11. Structures of μ-oxo diiron(III) porphyrazine complexes.

A series of μ-bridged diiron complexes supported by octapropylporphyrazine ligands $[FePz(n\text{-}C_3H_7)_8)_2X$ (X = O, N, C) was prepared and structurally characterized [76]. In contrast to μ-oxo diiron(III) complex, the Fe^{IV}=C=Fe^{IV} and Fe^{III}-N=Fe^{IV} species crystallized with one C_6H_6 molecule per two dimers arranged cofacially via π–π interaction due to their higher Lewis acidity. The Fe-X-Fe angle increases in the series μ-oxo - μ-nitrido - μ-carbido from 158.5° to 168.5° and 175.1°, respectively, according to the Fe-X bond order. Nevertheless, the Fe-X bond lengths don't follow this tendency: Fe-O = 1.75/1.76 Å > Fe-C = 1.67/1.67 Å > Fe-O = 1.65/1.66 Å. According to DFT calculations, unexpectedly long Fe-C bond was explained by back π–donation from μ-C group to the Fe-C antibonding orbital. The positions of the pre-edge maxima in the XANES spectra are in agreement with the expected order 7115.6 (μ-C) > 7113.8 (μ-N) > 7112.9 (μ-O) eV. UV-vis spectra suggest the stronger interaction of the two porphyrazine ligands in μ-carbido and μ-nitrido complexes in agreement with their shorter distances between macrocycles. Nevertheless, the nature of the bridging group does not influence the relative orientation of the porphyrazine macrocycle in the dimeric molecules. Staggering angles of 24.2, 26.2 and 24.2° were found in μ-oxo, μ-nitrido and μ-carbido diiron porphyrazine complexes, respectively [76].

μ-Oxo diiron(III) (ethylthio)porphyrazine complex $[FePz(SC_2H_5)_8]_2O$ can be prepared by passing mononuclear precursor through the column with basic Al_2O_3 [77]. The IR spectrum of $[FePz(SC_2H_5)_8]_2O$ showed new features in region 800-900 cm^{-1} due to the expected Fe-O-Fe stretching as well as at 695, 951 and 1104 cm^{-1} which were absent in the IR spectrum of monomeric precursor. The electrochemical properties of $[FePz(SC_2H_5)_8]_2O$ were quite different from those of porphyrin and phthalocyanine counterparts. The cyclic voltammogram exhibited two oxidation steps at $E_{1/2}$ = 0.37 and 0.62 V (vs SCE) and four reduction events at $E_{1/2}$ = -0.26, -0.48, -0.92 and -1.30 V. This redox behaviour is very different from those of $(TPPFe)_2O$ and $(PcFe)_2O$ but the electronic and structural origin of this difference is not yet understood [77].

2.4. Corroles

2.4.1. Iron

Corrole complexes attract a significant attention due to their distinctive structural and electronic properties [78]. Several μ-oxo corrole complexes have been reported. Diamagnetic

μ-oxo diiron complex supported by corrole ligands bearing C_6F_5 substitients was published by Gross and co-workers (Fig. 12) [79].

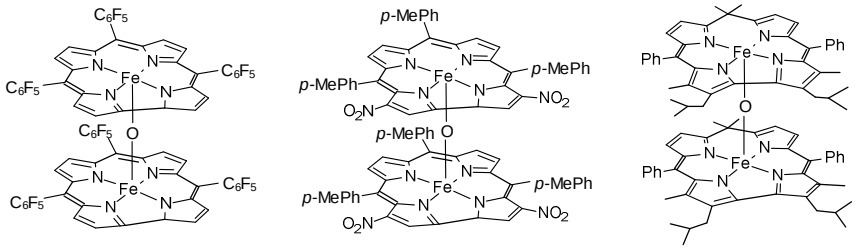

Fig. 12. Structures of μ-oxo diiron 5,10,15-tris(pentafluorophenyl)corrole, $(FePFPC)_2O$, μ-oxo diiron 3,17-dinitro-5,10,15-triphenylcorrole, $[FeTPC(NO_2)]_2O$, and μ-oxo diiron 13,16-di-*iso*-butyl-10,19-diphenyl-5,5,12,17-tetramethylisocorrole, $(FeIC)_2O$.

Since corroles are trianionic tetradentate ligands, the iron sites in their μ-oxo dimers are formally in Fe(IV) oxidation state. The electronic structure of four μ-oxo diiron *meso*-tris(*para*-X-phenyl)corrole complexes (X = H, OCH_3, CH_3, CF_3) was determined by UV-vis and Raman studies and supported by DFT calculations [80]. The iron sites in these complexes were proposed to be intermediate-spin Fe(III) coupled to corrole radicals rather than previously proposed Fe(IV) sites in $(Fe^{IV}TPC)_2O$ formulation.

The coordination of the iron atom in μ-oxo diiron 3,17-dinitro-5,10,15-triphenylcorrole $[FeTPC(NO_2)]_2O$ is square pyramidal with out-of-plane iron withdrawal of 0.383 and 0.385 Å with short Fe-O lengths (1.709 and 1.713 Å) [81]. The Fe-O-Fe angle is 170.89° leading to small dihedral angle between two N_4 plane (7.38°). Two corrole macrocycles are rotated 60.0° from the eclipsed conformation.

The most important structural data of available corrole μ-oxo dimers are listed in Table 1.

Table 1. Structural parameters of μ-oxo metal corrole complexes. Bond lengths are given in Å.

Complex (ref)	M-O-M angle	M-O_{bridge}	M out-of-plane distance	Interplane distance	M-$N_{pyrrole}$	Staggering angle
$[FeTPC(NO_2)]_2O$ [81]	170.89°	1.709 1.713	0.383 0.385	4.19	1.898 – 1.922	60°
$(FePFPC)_2O$ [79]	158°	1.709 1.726	0.421 0.426	4.28	1.884 - 1.929	n.d.
$(FeIC)_2O$ [82]	172.6°	1.761	0.615	4.75	2.001 – 2.012	n.d.

$(SiPFPC)_2O$ [83]	164.4°	1.615 1.616	0.402 0.407	4.04	1.841 – 1.856	90.3°
$(GeTPC)_2O$-1 [84]	149.0°	1.735 1.751	0.425 0.449	4.36	1.900 - 1.924	n.d.
$(GeTPC)_2O$-2 [84]	147.3°	1.718 1.773	0.441 0.441	4.37	1.881 – 1.930	n.d.

[$TPC(NO_2)$] - 3,17-dinitro-5,10,15-triphenylcorrole; TPC = triphenylcorrole

μ-Oxo diiron complex was also prepared using isocorrole platform by the treatment with aqueous NaOH solution (Fig. 10) [82]. This tetrapyrrolic ligand has two internal N-H groups and quite different HOMO and LUMO energy levels compared to corrole counterpart. Although the nitrogen σ–donor strength is weaker and metal-nitrogen π–bonding is different, the coordination geometry of iron is similar to corrole and porphyrin complexes. The lengths of Fe-O bonds are 1.761, 1.754 and 1.705 Å and the Fe-O-Fe angles are 172.6, 172.2 and 170.1° for isocorrole, porphyrin and corrole μ-oxo dimers, respectively. However, the iron withdrawal from N_4 isocorrole plane is significantly greater for isocorrole μ-oxo dimer (0.615 Å) with respect to porphyrin and corrole analogs (0.484 and 0.407 Å, respectively) [82].

2.4.2. Silicon

While a number of μ-oxo disilicon phthalocyanines have been studied due to their promising optoelectronic properties arising from electronic interaction between the two macrocycles [51-56], the access to their corrole analogs was not developed until recently. The first Si(IV) corrole complexes prepared from of *meso*-triarylcorroles and $SiCl_4$ were converted to μ-oxo dimeric complexes by treatment with methanesulfonyl chloride in Py at 100° [83]. The ^{19}F NMR signals of the *ortho*- and *meta*-fluorine atoms of $(SiPFPC)_2O$ split indicating non-equivalence of upper and lower F with respect to corrole plane. Comparison with other known μ-oxo corrole complexes $(FePFPC)_2O$ [79] and two forms of $(GeTPC)_2O$ [84] (TPC = triphenylcorrole) shows a shorter Si-O distances of 1.615 and 1.616 Å with respect to 1.709/1.726 Å, 1.735/1.751 Å and 1.718/1.773 Å, respectively (Table 1). This provides a stronger orbital overlap in $(SiPFPC)_2O$. The Si-O-Si angle of 164.44° is bigger than corresponding angles in Fe-O-Fe (158.0°) and Ge-O-Ge (149.0° and 147.3°) units. The mean distances between two corrole planes are 4.04 Å for $(SiPFPC)_2O$, 4.28 Å for $(FePFPC)_2O$ and 4.36/4.37 Å for $(GeTPC)_2O$. In contrast to Fe and Ge μ-oxo dimers, the corrole cycles in $(SiPFPC)_2O$ are twisted by 90.3°. This twisted conformation should be the most stable according to DFT calculations.

2.5. Tetrabenzotriazacorroles

2.5.1. Phosphorus

A μ-oxo dimer of phosphorus(V) tetrabenzotriazole was prepared in a low yield according to the synthetic route depicted in Scheme 1 [85].

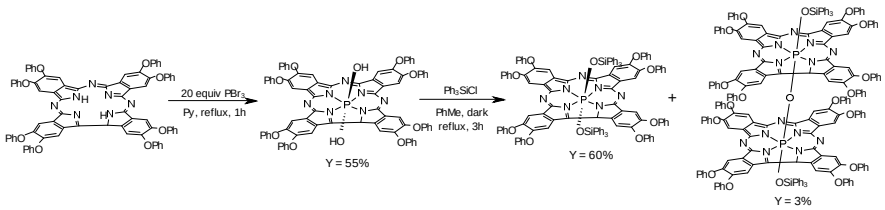

Scheme 1. Preparation of μ-oxo dimeric phosphorus(V) tetrabenzotriazacorrole.

The ^{1}H and ^{31}P NMR spectra of this μ-oxo dimer showed one set of signals of tetrabenzotriazacorrole cycle shifted to higher field with respect to monomer precursor even at low temperature. The absorption band of the μ-oxo complex in $CHCl_3$ solution are broadened and blue-shifted from 451 and 662 nm for monomer to 425 and 635 nm for dimer, respectively. The energy difference between optimized dimeric structures was less than 4 kcal mol^{-1} resulting in a rapid rotation of two macrocycles of μ-oxo dimer which is in agreement with NMR data.

2.6. Contracted porphyrinoids

Recent interest in subphthalocyanines and subporphyrins has been stimulated by their unusual properties arising from their smaller macrocyclic π–conjugation system [86]. In contrast to the planar tetrapyrrolic phthalocyanine macrocycle, the three isoindole fragments of subPc form a non-planar bowl shape providing their particular properties. For instance, subphthalocyanines exhibit intense fluorescence and unusual nonlinear optical properties. For a long time, the access to $(subPcB)_2O$ and its substituted derivatives was based on the self-condensation of subPcB-OH or its reaction with subPcB-Cl to furnish μ-oxo dimer in milligram amounts [87,88]. Bender and co-workers [89] in parallel with Yamasaki and Mori [90] have recently developed a gram scale synthesis of homoleptic and heteroleptic μ-oxo subphthalocyanines. After thorough evaluation of different routes, it was concluded that the reaction of equimolar amounts of subPcB-OH and subPcB-Br in CH_2ClCH_2Cl in the presence of K_3PO_4 was the most efficient and reproducible procedure to synthesize $(subPcB)_2O$ in

gram amounts [89]. After Soxhlet extraction, Kaufmann column chromatography and train sublimation, ~30% yields of pure, doubly sublimated μ-oxo dimer were obtained. This synthetic methodology was successfully applied for the preparation of three heteroleptic derivatives (Scheme 2).

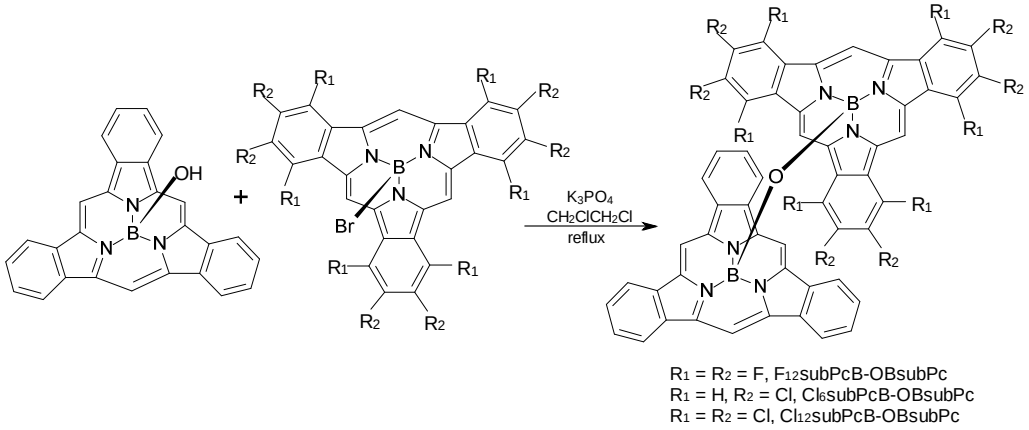

Scheme 2. Preparation of heteroleptic μ-oxo dimers F_{12}subPcB-O-BsubPc, Cl_6subPcB-O-BsubPc and Cl_{12}subPcB-O-BsubPc.

The optical absorption with considerable blue-shift and fluorescent properties of these μ-oxo dimers differ significantly from those of regular subPcB complexes. The crystal structures of non-solvated $(subPcB)_2O$ and its two solvated forms were investigated in great details [91]. Depending on the crystal composition, the B-O-B angles of 130.6, 132.8 and 133.6° were observed. The crystals obtained by sublimation were highly symmetric and of unusually high density for subphthalocyanine derivative of any type allowing for π–π intermolecular interaction which makes it very attractive as functional material.

μ-Oxo subporphyrin species are much less investigated compared to their subphthalocyanine congeners [92,93]. To access μ-oxo *meso*-phenyl subporphyrin complexes Kobayashi and coworkers heated axially hydroxyl-substituted subporphyrin in vacuum in the presence of Et_3N (Scheme 3).

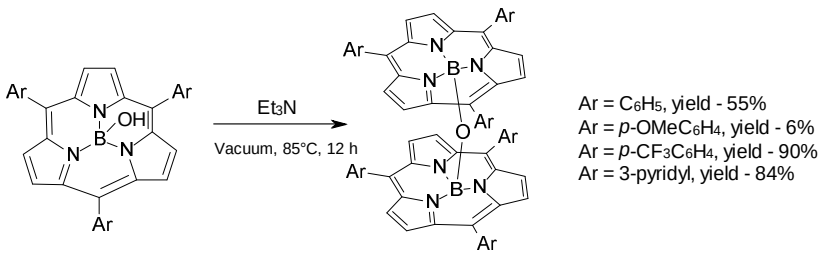

Scheme 3. Preparation of µ-oxo dimeric subporphyrins.

Substitution pattern at meso-aryl subporphyrin groups influenced the yields of µ-oxo dimers. The higher yields (up to 90%) were obtained from subporphyrins bearing electron-withdrawing groups due to increased Lewis acidity of the boron atom. The single-crystal X-ray diffraction analysis of phenyl substituted µ-oxo dimer showed a bent B-O-B fragment with an angle of 139.6° with two ligands twisted by ~33° owing to steric hindrance of *meso*-phenyl groups.

Similarly, a heterotrimer of silicon phthalocyanine bearing two *meso*-aryl subporphyrin unit, (subporphyrin)B-O-Si(Pc)-O-B(subporphyrin) was prepared at 120°C and characterized by MALDI-TOF mass and ^{1}H NMR spectra. However, this trimer suffered from low stability during isolation giving rise µ-oxo heterodimer and mononuclear complexes. A µ-oxo-connected (SubPc)B-O-P(tetrabenzotriazacorrole)-O-B(SubPc) was prepared from subphthalocyanine with axial chlorine and phosphorus(V) tetrabenzotriazacorrole by the treatment with AgOTf in PhMe for 1 h at room temperature followed by reflux in the presence of $NEt^{i}Pr_2$ for 3 h [94]. This trimer absorbs light across the entire UV-vis region. Another stable µ-oxo heterodimer was synthesized from dihydroxylisicon 1,4,8,11,15,18,22,25-octakis(hexyl)phthalocyanine and chloroboron subphthalocyanine [54].

2.7. µ-Oxo dimers supported by covalently linked macrocycles

The µ-oxo bridged binuclear complexes where two porphyrin moieties are connected by different linkers have received much attention in recent years [95-101]. Several such constructions with flexible and rigid linkers were structurally characterized (Fig. 13).

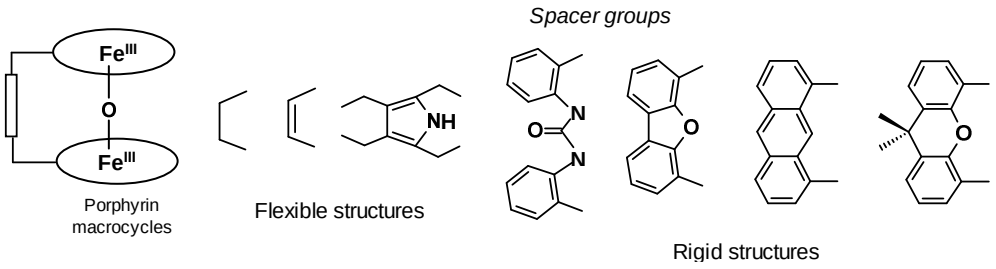

Fig. 13. Structurally characterized µ-oxo diiron complexes with linked porphyrin ligands [57].

The different aspects of the chemistry of these constructions were described in details in the recent review by Rath and co-workers [57]. Here we highlight the most important features of these diiron(III) high-spin (S = 5/2) systems and further information can be found in ref. 57. Ethane, ethene and pyrrole linkers provide the dimeric structures with a significant flexibility. The conformational switching between closed and open forms is readily triggered by the addition of base or acid accompanied by the distinctive colour changes. X-ray structures of these μ-oxo species exhibit cofacial arrangement of porphyrin macrocycles with considerably bent Fe-O-Fe fragments: 147.9, 150.9 and 151.97° for ethane, ethene and pyrrole bridged complexes, respectively. The porphyrin macrocycles are more distorted compared to unlinked counterparts with short Fe-Fe distances (3.409, 3.453 and 3.454 Å) and mean plane separations (4.33, 4.51 and 4.54 Å) for for ethane, ethene and pyrrole bridged complexes, respectively. More rigid aromatic spacers of covalently linked μ-oxo dimers (Fig. 10) lead to less bent structures with Fe-O-Fe angles of 165.7 – 174.8° and longer Fe-Fe distances (3.491-3.511 Å) and mean plane separations (up to 4.74 Å) [57]. Two iron(III) sites in the ethane- and pyrrole-bridged μ-oxo complexes are strongly antiferromagnetically coupled: J = - 126.6 cm^{-1} [98] and J = - 137.7 cm^{-1} [101], respectively. Thus, the structural tuning of μ-oxo diiron structure allows for precise control of the interaction and electronic communication between porphyrin cycles. Interestingly, the protonation of linked μ-oxo diiron porphyrin complexes by strong acids with weakly coordinated anions (e.g. ClO_4^-, BF_4^-, PF_6^-, SbF_6^-) in CH_2Cl_2 provides access to corresponding μ-hydroxo species [57,101]. Upon protonation, the Fe-OH-Fe angle becomes more bent and two porphyrin planes further approach each other. Their increased interaction leads to unequally distorted porphyrin cores resulting in two different iron spin states in the μ-oxo dimer molecule [102]. The nature and size of anion also affects on the iron spin state due to the interaction with the hydroxyl group and iron sites. The calculations indicated that subtle environmental perturbations strongly influence the spin state of iron atoms [98]. Protonation of μ-oxo group of pyrrole bridged dimer resulted in decrease of coupling constants to J = - 42.2 cm^{-1} (with HBF_4), J = - 44.1 cm^{-1} (with $HSbF_6$) and (with HPF_6) [101]. These coupling constants are greater than those for μ-hydroxo complexes of ethane-bridged complexes: J = - 36, 36.5 and 37.6 cm^{-1} for the complexes protonated by HBF_4, $HSbF_6$ and HPF_6, respectively [101]. The increase of the Fe-O bond length was proposed to be the key factor for the decrease of J, whereas Fe-O-Fe angle and the presence of proton play only a secondary role [96]. In sharp contrast, ethane-bridged μ-hydroxo dimanganese octaethylporphyrin bears two equivalent high-spin Mn(III) sites

[100]. Small molecules of organic solvents such as H_2O, C_6H_6, PhMe, THF, etc. can be accommodated in the cavity between porphyrin planes [57].

3. Photocatalytic generation of high-valent metal oxo species starting from µ-oxo dimers

µ-Oxo bimetallic complexes can be used for photochemical generation of mononuclear high-valent oxo species via photodisproportionation of the M-O-M fragment upon direct excitation into the oxygen-to-iron charge transfer (Fig. 14).

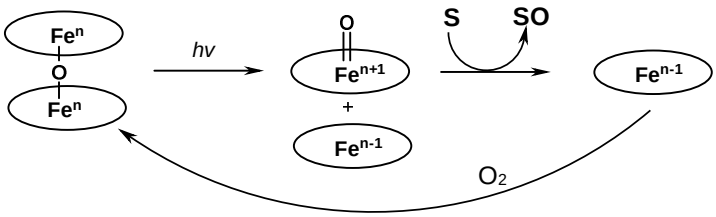

Fig. 14. Schematic representation of the catalytic photooxidation cycle involving µ-oxo diiron complexes.

Although the quantum yields are not high because of the recombination of Fe(IV)=O and Fe(II) to reform the parent µ-oxo diiron complex, this route can allow using O_2 as the clean oxidant without added reductants to develop clean oxidation catalytic processes. Different metals (Fe, Mn, Ru) in combination with several porphyrinoid ligands have been used to perform this chemistry. Covalent linking of macrocycles resulted in the improvement of the catalytic properties. Nocera and co-workers have developed this approach using different Pacman iron porphyrins [103-105]. Photon absorption by the diiron(III) µ-oxo chromophore resulted in the Fe-O-Fe photocleavage to form PFe^{IV}=O and PFe^{II} pair (Fig. 15).

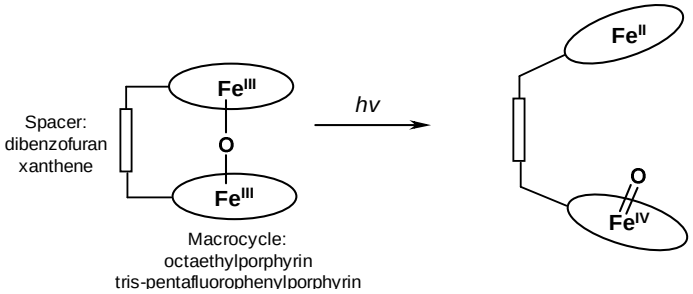

Fig. 15. Photogeneration of iron oxo species from iron Pacman porphyrins.

The Pacman construction shows a significant vertical flexibility: while iron-iron distance in μ-oxo form is about 3.5 Å, it increases to > 7.5 Å in the relaxed pocket which makes possible the approach of substrate to oxo species. Electron-withdrawing groups at macrocycles increase oxidizing properties of photogenerated PFe^{IV}=O species. Pacman diiron porphyrin with pentafluorophenyl substituents catalyzes aerobic photooxidation of olefins with high turnover numbers (Fig. 16) [104].

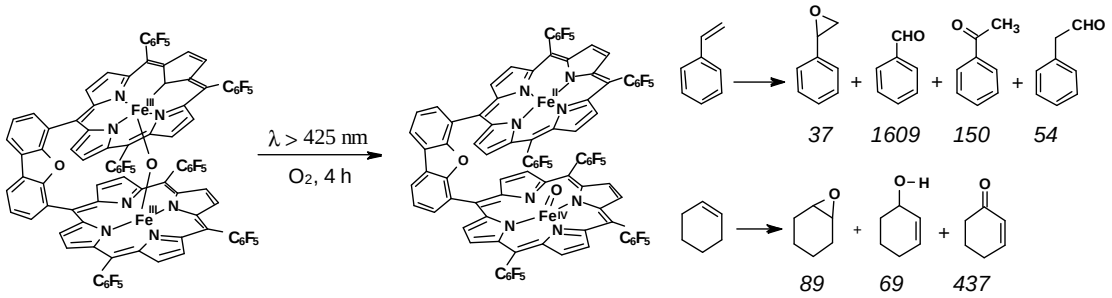

Fig. 16. Aerobic photooxidation of olefins mediated by μ-oxo Pacman diiron porphyrin with pentafluorophenyl groups. The product amounts are in TONs.

The product distribution of cyclohexene and styrene oxidation was typical for radical processes. Noteworthy, *cis*-cyclooctene and *cis/trans*-stylbenes did not react under photocatalytic conditions owing to the inability of bulky substrates to access the sterically hindered cleft of the Pacman architecture [104]. Comparison of catalytic activity of covalently linked and unlinked μ-oxo diiron species in the photooxidation of dimethylsulfide showed 9635 and 688 turnovers, respectively, indicating a higher efficiency of the Pacman complex. These findings demonstrated a beneficial effect of the covalently linked μ-oxo diiron scaffold. The scope of this approach was extended to the aerobic photooxidation of hydrocarbons with activated C-H bonds (Table 2) [105].

Table 2. Aerobic photooxidation of hydrocarbons in the presence of μ-oxo diiron fluorinated Pacman porphyrin. Conditions: λ = 425 nm, 1 atm O_2, 25°C, 18 h [105].

Substrate (BDE_{C-H}, kcal/mol)	Product	Turnover number
Fluorene (80)	fluorenone	287
Dihydroanthracene (84.5)	anthracene	235
Diphenylmethane (84.8)	benzophenone	160
Cumene (90)	acetophenone	143

	cumyl alcohol	116
Toluene (90)	benzaldehyde	76

μ-Oxo diiron (IV) complex $(FePFPC)_2O$ with corrole macrocycle which stabilizes higher metal oxidation states provided a rare access to a putative Fe^{V}=O species rather than to Fe^{IV}=O entity generated from μ-oxo diiron(III) porphyrin complexes. Photoactivation of $(FePFPC)_2O$ by laser irradiation with λ = 355 nm generated Fe^{III}PFPC and oxo species formulated as $PFPCFe^{V}$=O on the basis of its higher reactivity in the oxidation of ethylbenzene with respect to PFe^{IV}=O and $(P^{+\cdot})Fe^{IV}$=O and k_H/k_D value of 3.6 [106]. $PFPCFe^{V}$=O reacted with *cis*-cyclohexene, dihydroantracene, cumene, ethylbenzene and toluene with the second-order rate constants in the range of $4 \times 10^2 - 5.4 \times 10^3$ M^{-1} s^{-1}. Radical scavenger N-*tert*-butyl-phenylnitrone had small effect on the formation of *cis*-cyclooctene oxide [107]. $[Fe^{III}(TPP)]_2O$ and $Ru^{IV}(TMP)O_2$ showed lower catalytic acitivities under the same conditions. *cis*-Cyclooctene was photooxidized to *cis*-cyclooctene oxide with TON ~ 200 after 48 h of irradiation with 400-500 nm light in the presence of air [107]. The oxidation of norbornene afforded the corresponding epoxide with TON = 72 after 24 h of photolysis whereas allylic oxidation products 2-cyclohexenol and 2-cyclohexenone were obtained in the oxidation of cyclohexene with TON of 230 and 102, respectively, along with minor amount of the epoxide (TON = 40). Activated hydrocarbons such as Ph_3CH, Ph_2CH_2, PhEt and xanthene were oxidized to the corresponding alcohols and ketones with TON ~ 80 – 1200 [107]. This system was also active in the aerobic oxidation of secondary benzylic alcohols.

In the case of heteroleptic μ-oxo dimer complex with two non-equivalent iron sites two isomeric high-valent oxo species can be formed. A mixted μ-oxo bridged heme/non-heme diiron complex was prepared by Karlin and co-workers and photooxidation of different substrates was studied [108]. Low temperature transient absorption spectroscopy investigation indicated the formation of ferrous porphyrin and high-valent oxo species at non-heme iron (Fig. 17).

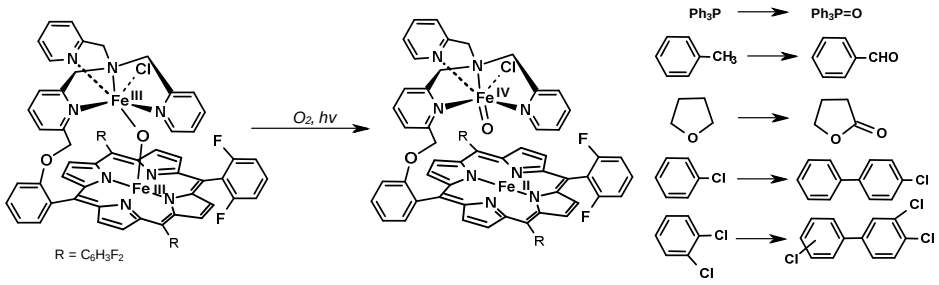

Fig. 17. Photogeneration of non-heme Fe^{IV}=O from heteroleptic μ-oxo complex and its reactivity.

This species carried out the oxidation of tetrahydrofuran and toluene solvents in anaerobic single-turnover conditions with 15 and 23 % yields of γ–butyrolactone and benzaldehyde, respectively. When photolysis was performed under aerobic conditions, the oxygen transfer to Ph_3P provided TON = 28 before degradation of the complex. The photolysis of the heteroleptic μ-oxo diiron complex in chlorobenzene or 1,2-dichlorobenzene led to C-Cl cleavage reactions to form monochlorobiphenyls or trichlorobiphenyls, respectively. The non-heme Fe^{IV}=O is most likely responsible for the C-H bond cleavage and subsequent radical chemistry.

Although Mn-O-Mn bonds are relatively weak in dimeric macrocyclic complexes and can be dissociated in polar solvents, μ-oxo dimanganese complexes are quite stable in non-polar solvents, e.g. benzene or cyclohexane [109]. Due to decrease of the electron density at metal sites, F and CF_3 electron-withdrawing substituents on the porphyrin core favor the formation of μ-oxo dimers. Visible light photolysis of $(TPPMn)_2O$ and related $(4\text{-}F\text{-}TPPMn)_2O$ and $(4\text{-}CF_3\text{-}TPPMn)_2O$ complexes produced (Porphyrin)Mn^{IV}=O and (Porphyrin)Mn^{II} species. The latter is rapidly oxidized to Mn^{III} porphyrin in the presence of O_2. Otherwise, (Porphyrin)Mn^{II} can be stabilized in the presence of Py or PPh_3 forming (Porphyrin)Mn^{II}(Py) or (Porphyrin)$Mn^{II}(PPh_3)$ complexes, respectively. Upon addition of cyclohexene or styrene the (Porphyrin)Mn^{IV}=O species were transformed to Mn^{III} porphyrin complexes indicating the oxidation of the olefins. However, the product composition has not been published.

In search of photocatalysts capable of performing more demanding oxidation of alkanes, several μ-oxo diruthenium(IV) porphyrin complexes have been evaluated [110]. The UV-vis spectra showed that photocatalytic cleavage of $[TPPRu^{IV}(OH)]_2O$ and $TPPRu^{III}$ – pyridinium N-oxide adduct provided the same oxo species $TPPRu^{V}$=O [111]. Laser flash photolysis studies allowed for determination of second-order rate constants: $k_2 = 6.6 \times 10^3\ M^{-1}\ s^{-1}$ (diphenylmethanol), $k_2 = 2.5 \times 10^3\ M^{-1}\ s^{-1}$ (styrene), $k_2 = 1.8 \times 10^3\ M^{-1}\ s^{-1}$ (cyclohexene). Among complexes with different substitution pattern, $[Ru^{IV}(p\text{-}CF_3\text{-}TPP)OH]_2O$ exhibited the highest turnover numbers in the oxidation of hydrocarbons (Fig. 18, Table 3).

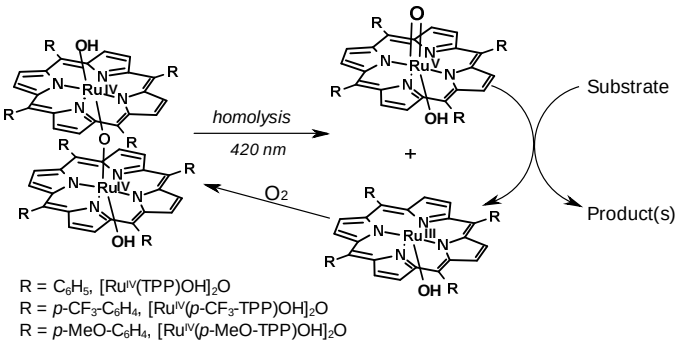

Fig. 18. Photocatalytic oxidation of substrates in the presence of μ-oxo diruthenium(IV) porphyrin complexes.

Table 3. Photocatalytic oxidation of olefins and benzylic compounds in the presence of $[Ru^{IV}(p\text{-}CF_3\text{-}TPP)OH]_2O$.

Entry	Substrate	Products	Turnover number
1	Norbornene	Norbornene oxide	200
2	Cyclohexene	2-Cyclohexenol 2-Cyclohexenone Cyclohexene oxide	160 350 30
3	Triphenylmethane	Triphenylmethanol	1120
4	Diphenylmethane	Diphenylmethanol Benzophenone	820 140
5	Ethylbenzene	1-Phenylethanol Acetophenone	380 180
6	Xanthene	9-Xanthone	2900
7	1-Phenylethanol	Acetophenone	3300
8	9-Xanthenol	9-Xanthone	3900

The catalytic efficiency expressed in turnover numbers correlates with the order of substrate reactivity, i.e. with bond dissociation energies of C-H bonds. Kinetic isotope effect k_H/k_D = 4.8 ± 0.2 (25°C) measured in the competitive oxidation of ethylbenzene-h_{10} and ethylbenzene-d_{10} was in agreement with the involvement of oxo species [111]. μ-Oxo dimeric species can dissociate not necessarily under photoirradiation but also under catalysis conditions. For instance, the formation of $(PcF_{16})Fe^{III}$-O-$Fe^{III}(PcF_{16})$ was proposed in $FePcF_{16}$-catalyzed Wacker-type aerobic oxidation of the olefins to ketones which underwent monomerization upon interaction with triethylsilane [112].

To summarize, photolyses of $[(Corrole)Fe]_2O$, $[(Porphyrin)Mn]_2O$ and $[(Porphyrin)Ru]_2O$ complexes indicated the similar reaction manifold in all cases. The formed oxo species are capable of oxidizing benzylic alcohols, olefins and activated hydrocarbons. The Pacman architecture of μ-oxo complexes leads to more efficient oxidation, but the overall efficiency depends on the ratio between the reaction rate with substrate and the life time of oxo species which is formed with τ_{open} = 20 ps and undergoes re-clamping to μ-oxo species with $\tau_{reclamp}$ = 1.3 ns [113].

4. Catalysis

4.1. Oxidation

Single atom bridged binuclear macrocyclic complexes have been regarded as inactive species in catalysis for a long time, but increasing number of their catalytic applications as well as some mechanistic considerations indicate their great interest for catalysis [32]. Since the activity of mononuclear porphyrin [4] and phthalocyanine [114,115] complexes in oxidation has been associated with high-valent iron oxo species their binuclear counterparts have been a subject of extensive research. High-valent μ-nitrido diiron oxo species with phthalocyanine [116], porphyrin [19,117] and porphyrazine [118] ligands have been prepared and spectroscopically characterized. As for high-valent diiron oxo species on μ-oxo platform, their involvement in the oxidation of the aromatic compounds was initially proposed on the basis of reactivity studies [10-12,119]. Recently, $(PcF_{16})Fe^{IV}$-O-$Fe^{IV}(PcF_{16})$=O species formed from $(PcF_{16})Fe^{III}$-O-$Fe^{III}(PcF_{16})$ and H_2O_2 was detected by ESI-MS technique [120]. These studies provide a basis for the utilization of μ-oxo binuclear complexes in the catalytic oxidation.

Heteroleptic μ-oxo heme-Fe^{III}-O-Cu^{II}(L) complexes have been developed by Karlin and coworkers as models of cytochrome c oxidase [121]. This terminal enzyme of the respiratory chain, catalyzing the reduction of O_2 to H_2O, is also involved in both endogeneous generation and metabolism of redox-active signaling molecule NO [122]. The structures of selected complexes are shown in Fig. 19.

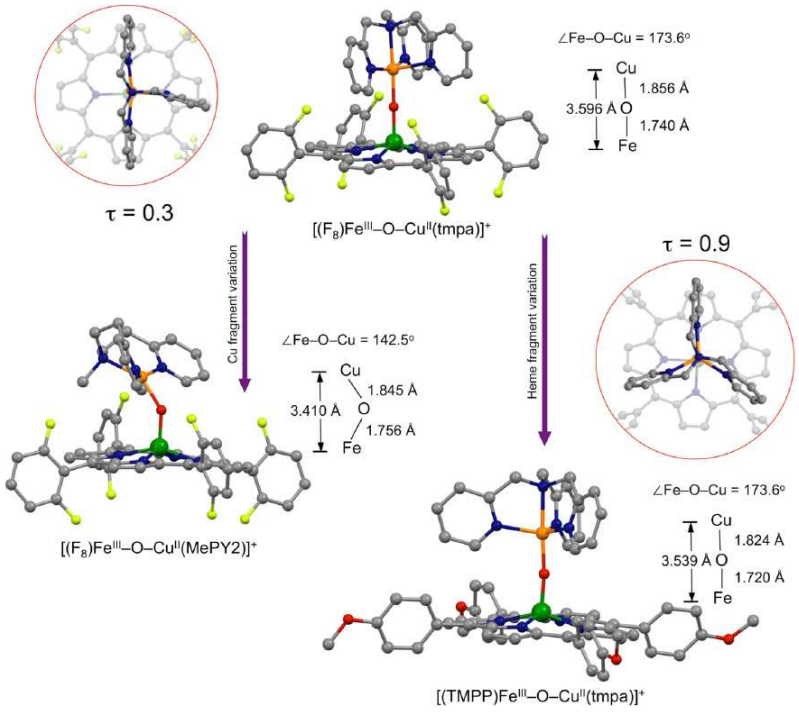

Fig. 19. Structures of (Porphyrinate)Fe^{III}-O-Cu^{II}(L) complexes. L = tmpa, tris(2-pyridylmethylamine); MePY2, bis(2-pyridyl-ethyl)methylamine. Porphyrinate = F_8, tetrakis(2,6-difluorophenyl)-porphyrinate; TMPP, tetrakis(4-methoxyphenyl)-porphyrinate. Reprinted with permission from Acc. Chem. Res. 48 (2015) 2462-2474. Copyright (2015) American Chemical Society.

The geometry of Fe-O-Cu core depends on the nature of Cu(II) site. While the involvement of tetradentate ligand for the Cu center led to near-linear Fe-O-Cu fragment, the complex bearing Cu(II) site with tridentate ligand exhibited a bent Fe-O-Cu unit with an angle of 142.5°. In turn, the electronic properties of porphyrin ligand determine the geometry of the heteroleptic binuclear complex. The cupric center of [(TMPP)Fe^{III}-O-Cu^{II}(tmpa)]$^+$ containing electron-donating porphyrin ligand adopts a nearly perfect trigonal bipyramidal geometry (τ = 0.9) whereas its counterpart [(F_8)Fe^{III}-O-Cu^{II}(tmpa)]$^+$ bearing electron-deficient porphyrin exhibits a distorted square pyramidal coordination (τ = 0.3) (Fig. 19). The bridging oxo group is very basic and can be protonated leading to bending of Fe^{III}-(OH)-Cu^{II} moiety and the elongation of Fe-O and Cu-O bonds. When Cu(II) site is coordinated with tridentate ligand, the μ-oxo ligand becomes (i) more basic and (ii) more accessible to favour the reaction with NO (Fig. 20).

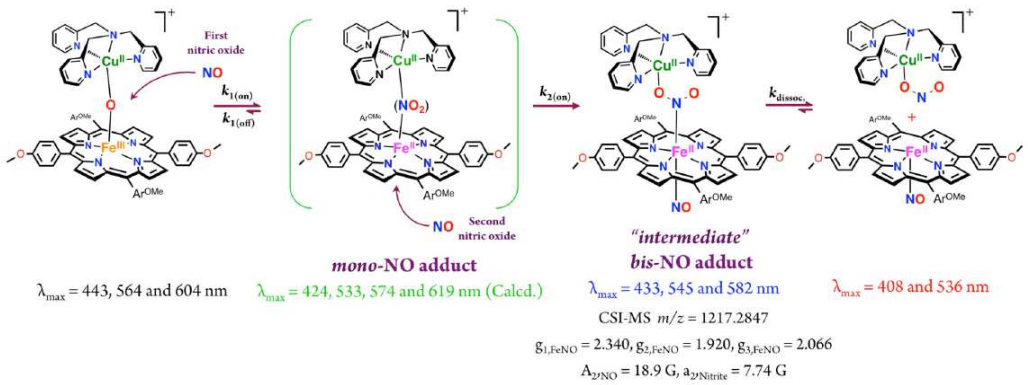

Fig. 20. Proposed mechanism of the oxidation of NO to nitrite mediated by µ-oxo heme-Fe^{III}-O-Cu^{II}(L) complexes. Reprinted with permission from Acc. Chem. Res. 48 (2015) 2462-2474. Copyright (2015) American Chemical Society.

The first NO molecule attacks the µ-oxo group followed by the addition of the second NO to ferrous porphyrin center. This bis-NO intermediate undergoes dissociation to release observed mononuclear cupric-nitrite and nitrosyl-ferrous heme complexes.

The $(FeTF_5PP)_2O$ complex was applied in the oxidative desulfurization process for the oxidation of dibenzothiophene and its derivatives considered as the most refractory sulfur compounds in fuels [61]. The model oil solution in octane contained 500 ppm of sulfur from each substrate, namely, dibenzothiophene (DBT), 1-benzothiophene (1-BT) and 4,6-dimethyldibenzothiophene (4,6-DMDBT). This solution was treated by H_2O_2 in the presence of 1 µmol $(FeTF_5PP)_2O$ and extracting solvent (MeCN, DMF, MeOH, 1-butyl-3-methylimidazolium hexafluorophosphate and tetrafluoroborate ionic liquids) at room temperature (Fig. 21).

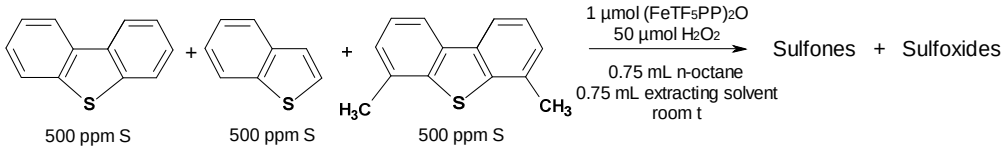

Fig. 21. Oxidation of model oil containing 500 ppm of sulphur from each benzothiophene derivative by $(FeTF_5PP)_2O$ – H_2O_2 system.

The sulfur compounds were extracted from oil by the polar solvent containing the catalyst and oxidant. Their oxidation to sulfones and sulfoxides led to continuous transfer of

sulfur compounds from the oil phase to extracting solvent resulting in the oil desulfurization. The catalytic efficiency followed the order 1-BT > DBT > 4,6-DMDBT whereas MeOH and MeCN were the optimal extracting solvents. Alternatively, the polar oxidized products can be also removed from fuels by absorption.

Interestingly, μ-oxo diiron tetrasulfophthalocyanine $(FePcS)_2O$ exhibited superior catalytic activity in the oxidative degradation of Orange II by ^tBuOOH in neutral aqueous solution in comparison with its μ-nitrido counterpart [123]. However, the stability of $(FePcS)_2O$ under catalytic conditions was very poor. In contrast to very stable $(FePcS)_2N$ complex, $(FePcS)_2O$ could not be used in the successive oxidations of Orange II. The significantly higher stability of $(FePcS)_2N$ compared to $(FePcS)_2O$ was also observed under strong acidic and strong basic solutions [124]. These binuclear species were reduced upon the reaction with sodium dithionite, thiourea dioxide, sodium hydroxymethanesulfinate and L-cystein.

Another fluorinated μ-oxo dimer was reported by Nemykin and co-workers [75]. μ-Oxo diiron(III) octakis(perfluorophenyl)tetraazaporphyrin was shown to be an efficient catalyst for the oxidation of aromatic compounds and aliphatic C-H bonds by hypervalent iodine compounds (PhIO, oligomeric iodosylbenzene sulphate $(PhIO)_3SO_3$) and $KHSO_5$. Peracetic acid has provided moderate product yields whereas the catalyst was inactive in the presence of H_2O_2. High yields of quinones were obtained in the oxidation of aromatic compounds using 1-2 mol % catalyst loading (Table 4).

Table 4. Oxidation of aromatic and aliphatic hydrocarbons by $[FeTAP(C_6F_5)_8]_2O$ – PhIO in CH_2Cl_2 at room temperature [75].

Entry	Catalyst amount (reaction time)	Substrate	Product (s), yields
1	2 mol % (2h)	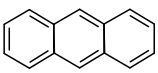	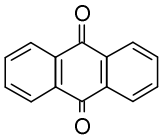 100 %
2	1 mol % (0.1 h)	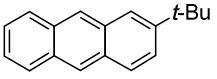	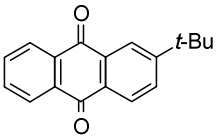 100 %

3	2 mol % (1 h)	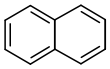	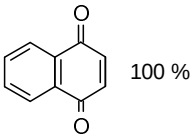 100 %
4	1 mol % (0.3 h)	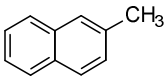	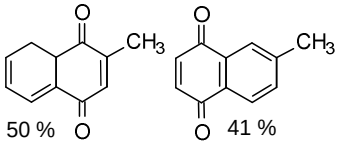 50 % 41 %
5	2 mol % (2 h)	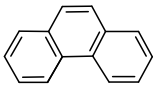	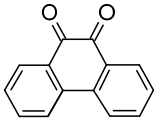 100 %
6	2 mol % (1 h)	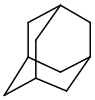	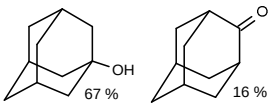 67 % 16 %
7	5 mol % (0.5 h)	$PhCH_3$	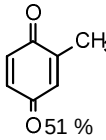 51 % PhCHO 26 % $PhCH_2OH$ 21 %

Importantly, a high yield (51 %) of 2-methylnaphthoquinone (vitamin K_3) was obtained in the demanding oxidation of 2-methylnaphthalene. Another interesting feature of $[FeTAP(C_6F_5)_8]_2O$ complex is a rare selectivity in the oxidation of toluene: 2-methylbenzoquinone was obtained with a 51 % yield whereas usual oxidation products PhCHO and $PhCH_2OH$ were minor oxidation products. Noteworthy, catalyst loading of 10-30 mol % of the related $(FePc^tBu_4)_2O$ complex should be used compared with 1-2 mol % of $[FeTAP(C_6F_5)_8]_2O$ to provide similar yields of products. Furthermore, $(FePc^tBu_4)_2O$ did not catalyze the oxidation of phenantrene, adamantane and toluene. In addition to increase of the catalytic activity, the fluorinated aromatic substituents confer to $[FeTAP(C_6F_5)_8]_2O$ a resistance to oxidative degradation allowing 8 consequitive oxidations of *tert*-butylanthracene using $(PhIO)_3SO_3$ oxidant [75]. The selective oxidation of anthracene to anthraquinone was carried out in the presence of 10 mol % of $(FePc^tBu_4)_2O$ and either 7.5 equiv. polymeric $(PhIO)_n$ or 2.5 equiv. oligomeric $(PhIO)_3SO_3$ [125]. The $(FePc^tBu_4)_2O$ complex in combination with $(Bu_4N)HSO_5$ was more efficient than with PhIO [126]. The oxidation of benzene, toluene, ethylbenzene, indane, 1,2,3,4,-tetrahydronaphthalene, 9,10-dihydroantracene, 2-methylnaphthalene, 2-*tert*-butylanthracene and anthracene furnished the corresponding *p*-quinones with 74-100% yields within 5-30 min in the presence of 6 equiv

$(Bu_4N)HSO_5$. Adamantane was also oxidized with 71% conversion to a mixture of alcohols and ketones.

μ-Oxo diiron tetraphenylporphyrin derivatives mediated a free-radical aerobic oxidation of cyclooctane, cyclohexane and cyclopentane to corresponding ketones and alcohols at 120°C [127]. Noteworthy, both electron-withdrawing (C_6F_5 > *p*-CF_3 > *p*-Cl) and electron-donating (*p*-CH_3 > *p*-OCH_3 > H) substituents at tetraphenylporphyrin ligand increased the catalytic activity.

Heterogeneous 2D coordination network material formed by (μ-oxo)bis[*meso*-tetrakis(*p*-carboxyphenylporphyrinato)iron(III)] complex (Fig. 8) exhibited moderate catalytic activity in the oxidation of benzyl alcohol (TON = 24), 1-phenylethanol (TON = 25), hexanol-1 (TON = 5) and octanol-1 (TON = 3) with ^{t}BuOOH [60]. FePcS inserted into nanocages of the metal organic framework MIL-100 mainly in μ-oxo form showed a superior catalytic efficiency in the oxidation of 2,3,6-trimethylphenol and 8-hydroquinoline to corresponding quinines compared with homogeneous mononuclear FePcS [128].

4.2. Nitrene transfer reactions

Ruthenium(IV) μ-oxo porphyrin complex $[Ru^{IV}(TPP)(OCH_3)]_2O$ prepared form $[Ru^{II}(TPP)(CO)(MeOH)$ and *m*-CPBA in MeOH promoted benzylic and allylic aminations as well as aziridination of aromatic olefins using 3,5-*bis*(trifluoromethyl)phenyl azide and *p*-*tert*-butylphenyl azide as nitrene sources (Fig. 22) [72].

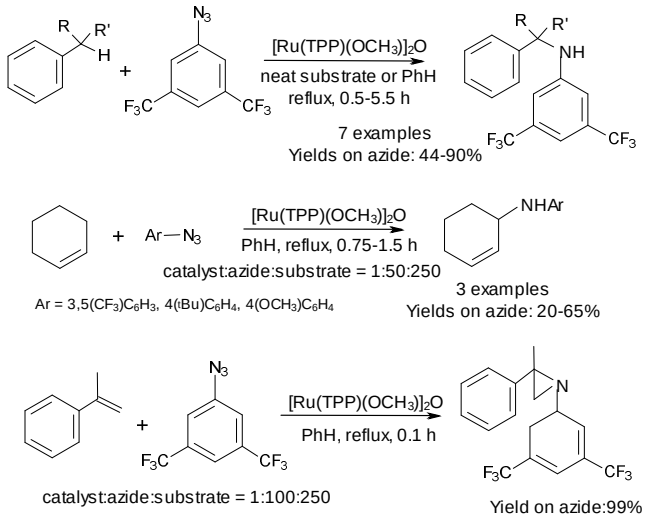

Fig. 22. Nitrene transfer reactions mediated by $[Ru^{IV}(TPP)(OCH_3)]_2O$ [72].

In the presence of 1-10 mol% catalyst with respect to limiting azide reagent, moderate to excellent yields of amination and aziridination products were obtained. Tosyl azide, adamantyl azide and benzyl azide were not suitable for this reaction. Since the observed catalytic activity of $[Ru^{IV}(TPP)(OCH_3)]_2O$ were similar to that of $Ru^{II}(TPP)(CO)$, it was proposed that μ-oxo dimer could be pre-catalyst and bis-imido complex $Ru^{IV}(TPP)(NAr)_2$ could be responsible for the catalytic activity. Interestingly, related $[Ru^{IV}(TPP)(m\text{-chlorobenzoate})]_2O$ complex did not react with 3,5-*bis*(trifluoromethyl)phenyl azide even under radiation.

4.3. Miscellaneous reactions

The $(TPPFe)_2O$ as well as $(salenFe)_2O$ complexes mediated the hydrophosphination of styrenes and acrylates with $HPPh_2$ and H_2PPh (Fig. 23) [129].

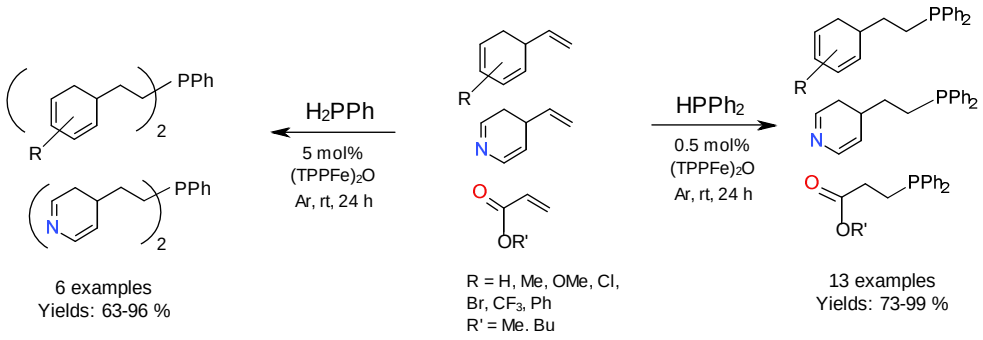

Fig. 23. Hydrophosphination of olefins with $HPPh_2$ and H_2PPh catalyzed by $(TPPFe)_2O$ [129].

This 100 % atom efficient and mild procedure (room T, solvent-free, non-toxic metal catalyst, no wastes) involves the addition of P-H bonds across a double bonds and provides access to important tertiary phosphines including unsymmetrically substituted derivatives.

The $(FePFPC)_2O$ complex in the presence of $(Ph_3P{=}N{=}PPh_3)Cl$ carried out copolymerization of cyclohexene epoxide, propylene oxide and glycidyl phenyl ether with CO_2 without the concomitant formation of olefin carbonates (Fig. 24) [130].

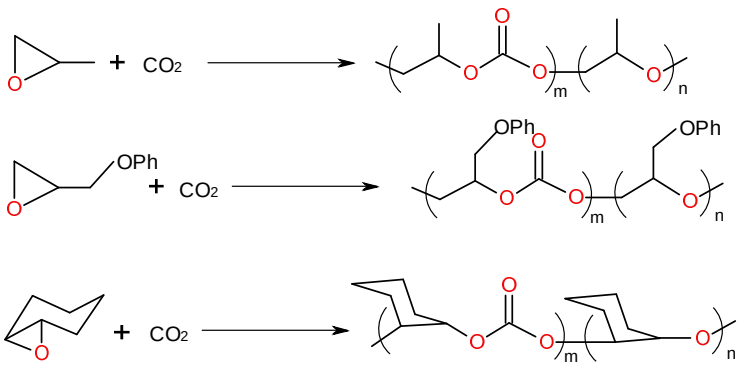

Fig. 24. Copolymerization of epoxides with CO_2 catalyzed by $(FePFPC)_2O$. Conditions: [epoxide] : $[(FePFPC)_2O]$: $[(Ph_3P{=}N{=}PPh_3)Cl]$ = 4000 : 1 : 1, P_{CO2} = 2 MPa, 60°C [130].

The propylene oxide copolymer containing minor amount of carbonate linkages (17 %) was obtained with high turnover frequency of 2008 mol of epoxide incorporated into the copolymer · (mol of catalyst)$^{-1}$ · h^{-1}. Mononuclear iron corrole complex showed lower catalytic activity [130].

5. Other applications

5.1. Optoelectronic applications

Incorporation of metal phthalocyanines in emerging optoelectrical applications in solar energy conversion and nonlinear optic systems attract much attention [131,132]. In this context, binuclear porphyrinoid complexes are particularly interesting since the optical and electronic properties can be advantageously modified [133]. There is a growing interest in the application of μ-oxo porphyrinoid complexes in optoelectronic devises. For example, the $(GaPc^tBu_4)_2O$ complex showed two-fold increase of saturation energy density and more intense photoluminescence emission in the red region compared to mononuclear $GaPc^tBu_4$ [134]. Basova and coworkers studied the formation of the thin ordered films of $(GaPc)_2O$ [135], $(AlPc)_2O$ [136] and $(AlPc^tBu_4)_2O$ [137] onto indium tin oxide, quartz slides, polished Si wafers and KBr. The mononuclear GaPc complex supported onto indium tin oxide by physical vapor deposition was transformed to ordered $(GaPc)_2O$ films in the presence of water upon annealing at ~300°C. X-ray photoelectron and Raman spectroscopies showed that as-deposited GaPc molecules exhibit the tilt angles between phthalocyanine plane and surface of 53 ± 5° whereas ordered $(GaPc)_2O$ molecules are oriented with the average tilt angles 85 ± 5°, i.e. practically perpendicular to surface. The surface-deposited AlPc complex undergoes transformation to corresponding μ-oxo species easier [135]. The well-organized $(AlPc^tBu_4)_2O$

films with elongated crystallites having preferential orientation were obtained upon heating of as-deposited $AlPc^tBu_4$ films in magnetic field whereas annealing with no magnetic field applied did not provided any effect on the morphology of the films. Magnetic field parallel to the support surface improves the azimuthal order of crystalline domains with the $(AlPc^tBu_4)_2O$ molecules oriented perpendicularly to surface and so that their dipole moments oppose the direction of the magnetic field [137]. Ordered films are of great importance for photovoltaic and chemical detection applications. This approach is especially useful for the complexes bearing sterically demanding substituents such as tert-butyl groups.

The thin films of $[(HO)SiPc^tBu_4]_2O$ onto a ferromagnetic rare earth garnet $Bi_{0.8}Dy_{2.2}Fe_{4.3}Al_{0.7}O_{12}$ were used for the switching of magneto-optical signals of a ferromagnetic substrate by a selective laser irradiation of a grafted μ-oxo disilicon phthalocyanine [138]. The photothermal energy transfer from $[(HO)SiPc^tBu_4]_2O$ film to inorganic magnetic substrate was further investigated [139]. The generation of heat in active organic layers which dissipates toward inorganic support leads to performance degradation of optoelectronic devises, e.g. organic light emitting diodes (OLED) and organic solar cells. This work has provided a more detailed understanding of this problem dealing with photothermal energy transfer in organic-inorganic hybrid materials.

Since boron subphthalocyanines are materials of particular interest for organic photovoltaic devices, their μ-oxo derivatives also attract much attention due to their unusual properties [140]. Evaluation of the pairing of $(subPcB)_2O$ with established electron donating and electron accepting materials indicated that it was better suitable as an electron donating material in simple bilayer structures. Its photovoltaic efficiency was comparable with that of highly optimized (subPcB)Cl structures with potential to improve the performance of the latter.

Complexes with metals possessing a magnetic moment can show interesting conductor properties due to a strong interaction between the Pc π–electrons and the metal d-electrons [42]. $[MnPc(CN)]_2O$ was shown to be a single-component molecular conductor with semiconductor behavior. Due to strong π-d interaction $[MnPc(CN)]_2O$ exhibits the magnetiresistance effect which can be used for the development of single-component crystals. The $[(p\text{-}BrTPP)Fe)_2O$ complex has good third-order nonlinear optical (NLO) properties showing one order of magnitude larger two-proton absorption cross-section value compared to the monomer owing to the more extended conjugated electronic structure [59].

μ-Oxo bridged iron 5,10,15,20-tetrakis(N-methyl-4-pyridiniumyl)porphyrin was used to assemble gold nanoparticles into networks, where the complex provides a molecular bridge

that couples the particules to form a ~1.5 nm separation gap between them [141]. Linear extinction, surface-enchanced Raman Scattering spectroscopy and TEM showed that plasmonic nanoparticle networks were formed by electrostatic interaction and that the Fe-O-Fe fragment was orthogonal to the inter-particle axis.

5.2. Medical applications

Sessler and co-workers have published the binuclear μ-oxo bismuth(III) texaphyrin complex (Fig. 25) [142].

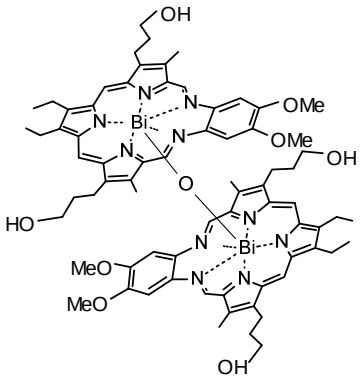

Fig. 25. Structure of μ-oxo dimeric Bi(III) texaphyrin.

The isotopes ^{212}Bi and ^{213}Bi with limited half-lives of 60.55 min and 45.65 min, respectively, are potentially useful as α–core emitters in the treatment of tumors but finding suitable ligands is a challenging task. In contrast to porphyrins showing selective localization in tumors but suffering from slow insertion kinetics and stability problems, this pentaaza expended porphyrinoid with ~20% larger cavity than the tetrapyrrolic congeners allows for fast Bi(III) insertion. Single-crystal structure of μ-oxo dimer show 2.194 Å Bi-O length with linear Bi-O-Bi unit and out-of-plane distance of the Bi(III) center of ~0.3 Å. This dimer is the first structurally characterized binuclear macrocyclic μ-oxo bismuth complex and the first stacked expanded porphyrin system prepared from a texaphyrin and a non-transition metal [142]. The corresponding monomeric complex obtained by the treatment with CF_3COOH in DMSO exhibited cytotoxic activity in the A2780 ovarian cancer cell line [142].

μ-Oxo diiron(IV) cationic *meso*(4-*N*-methylpyridyl)corrole interacts with DNA in a difunctional binding mode via non-classical intercalation and outside groove binding with H-aggregation with a higher binding constant than mononuclear analog, but shows a lower efficiency in the cleavage of supercoiled plasmid DNA in the presence of H_2O_2 or ^{t}BuOOH (Fig. 26) [143].

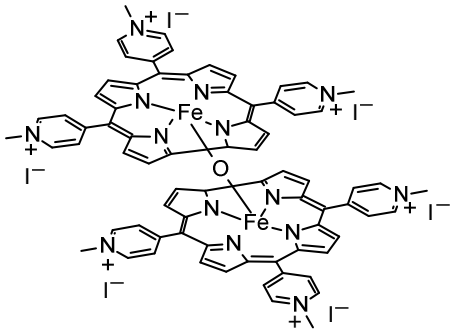

Fig. 26. Structure of μ-oxo diiron(IV) *meso*(4-*N*-methylpyridyl)corrole.

5.3. Miscellaneous

The ability of μ-oxo diiron porphyrins to undergo dissociation and reversible dimerization of mononuclear complexes upon changes in acido-basic conditions, solvent nature or the action of redox additives can be used for creating responsive polymer materials [144,145]. Two FeTPP moieties were connected by polystyrene or polyethylene oxide chains. The action of various stimuli resulted in the reversible formation of large macrocycles with μ-oxo diiron porphyrin polyethylene oxide repetitive units with intra- or intermolecular coupling depending on the concentration. This modification of the chain architecture can be useful for design of polymer systems with switchable properties.

The heterostructural C_3N_4@$(FeTPP)_2O$ material was prepared by adsorption of $(FeTPP)_2O$ onto graphitic carbon nitride due to π–π and iron-nitrogen interactions [146]. This composite material showed a significant enhancement in photocatalytic H_2 production under solar light. The high efficiency of the water reduction was explained by the action of $(FeTPP)_2O$ not only as photosensitizer, but also as a charge promoter to prevent the recombination of the excited electrons and holes of the g-C_3N_4.

6. Conclusion

μ-Oxo binuclear porphyrinoid complexes continue to attract much attention due to their particular properties. This review provides a summary on recent progress in their synthesis and applications. Selected examples discussed above illustrate a great versatility of μ-oxo platform which can accommodate different metals and non-metals, e.g. Fe, Mn, Ru, Cr, Mo, Re, Al, Si, P, B in homo- or heterometallic arrangements. Moreover, porphyrin, phthalocyanine, porphyrazine, corrole, tetrabenzotriazacorrole and their analogs can support

μ-oxo structure affording various homoleptic and heteroleptic constructions. In addition to tetrapyrrolic macrocycles, μ-oxo dimers of contracted and even expanded analogs can be prepared. The two macrocycles of μ-oxo complexes can be additionally connected via different covalent linkages [57,95-105] or via non-covalent interactions [37,46] to tune their structural and electronic properties. The syntheses and studies of various dimeric complexes based on different macrocycles via different linkages confirm the interest to binuclear constructions [147-151]. The important recent trend is the use of μ-oxo bimetallic scaffold for the construction of structurally organized solid materials [42,60,65]. The wealth of μ-oxo binuclear structures with very different properties explains their increasing utilization in very different areas: catalysis, sensors, optoelectrical and medical applications. Further studies and deeper understanding of their properties are likely to uncover many additional applications of μ-oxo binuclear complexes. Continued synthetic advances should provide a great variety of novel μ-oxo binuclear porphyrinoid complexes with divers properties opening the way for novel applications in catalysis and material science.

Acknowledgements

This work was supported by the Agence Nationale de la Recherche (ANR, France) (ANR-16-CE29-0018-01.

References

[1] Floris, B.; Donzello, M. P.; Ercolani, C. Single-Atom Bridged Dinuclear Metal Complexes with Emphasis on Phthalocyanine System. In *The Porphyrin Handbook*; Kadish, K. M., Smith, K. M., Guilard, R., Eds., Academic Press: Amsterdam, 2003, Vol. *18*, p 1-62.

[2] A.B. Sorokin, Adv. Inorg. Chem. 70 (2017) 107-169.

[3] V.N. Nemykin, I.N. Tret'yakova, S.V. Volkov, V.D. Li, N.G. Mekhryakova, O.L. Kaliya, E.A. Luk'yanets, Russ. Chem. Rev. 69 (2000) 325-346.

[4] M. Costas, Coord. Chem. Rev. 255 (2011) 2912-2932.

[5] A.B. Sorokin, Chem. Rev. 113 (2013) 8152-8191.

[6] E.N. Carrión, A. Loas, H.H. Patel, M. Pelmuş, K. Ramji, S.M. Gorun, J. Porphyrins Phthalocyanines 22 (2018) 1-27.

[7] I. Aviv-Harel, Z. Gross, Coord. Chem. Rev. 255 (2011) 717-736.

[8] M.S. Rodriguez-Morgade, P.A. Stuzhin, J. Porphyrins Phthalocyanines 8 (2004) 1129-1165.

[9] A.B. Sorokin, A. Tuel, New J. Chem. 23 (1999) 473-476.

[10] C. Pergrale, A.B. Sorokin, C. R. Chimie 3 (2000) 803-810.

[11] C. Pérollier, C. Pergrale-Mejean, A.B. Sorokin, New J. Chem. 29 (2005) 1400-1403.

[12] O.V. Zalomaeva, I.D. Ivanchikova, O.A. Kholdeeva, A.B. Sorokin, New J. Chem. 33 (2009) 1031-1037.

[13] M. Beyrhouty, A.B. Sorokin, S. Daniele, L.G. Hubert-Pfalzgraf, New J. Chem. 29 (2005) 1245-1248.

[14] O.V. Zalomaeva, A.B. Sorokin, New J. Chem. 30 (2006) 1768-1773.

[15] I.M. Geraskin,M.W. Luedtke, H.M. Neu, V.N. Nemykin, V.V. Zhdankin, Tetrahedron Lett. 49 (2008) 7410-7412.

[16] H.M. Neu, M.S. Yusubov, V.V. Zhdankin, V.N. Nemykin, Adv. Synth.Catal. 351 (2009) 3168-3174.

[17] D.S. Nesterov, O.V. Nesterova, A.J.L. Pombeiro, Coord. Chem. Rev. 355 (2018) 199-222.

[18] C. Colomban, E.V. Kudrik, P. Afanasiev, A.B. Sorokin, J. Am. Chem. Soc. 136 (2014) 11321-11330.

[19] E.V. Kudrik, P. Afanasiev, L.X. Alvarez, G. Blondin, M. Clémancey, J.-M. Latour, D. Bouchu, F. Albrieux, S.E. Nefedov, A.B. Sorokin, Nat. Chem. 4 (2012) 1024-1029.

[20] L.X. Alvarez, E.V. Kudrik, A.B. Sorokin, Chem. Eur. J. 17 (2011) 9298-9301.

[21] Ü. İşci, A.S. Faponle, P. Afanasiev, F. Albrieux, V. Briois, V. Ahsen, F. Dumoulin, A.B. Sorokin, S.P. de Visser, Chem Sci. 6 (2015) 5063-5075.

[22] Ü. İşci, P. Afanasiev, J.M.M. Millet, E.V. Kudrik, V. Ahsen, A.B. Sorokin, Dalton Trans. (2009) 7410-7420.

[23] E.V. Kudrik, P. Afanasiev, D. Bouchu, J.M.M. Millet, A.B. Sorokin, J. Porphyrins Phthalocyanines 12 (2008) 1078-1089.

[24] C. Colomban, E.V. Kudrik, P. Afanasiev, A.B. Sorokin, Catal. Today 235 (2014) 14-19.

[25] E.V. Kudrik, A.B. Sorokin, J. Mol. Catal. A: Chem. 426 (2017) 499-505.

[26] P. Afanasiev, A.B. Sorokin, Acc. Chem. Res. 49 (2016) 583-593.

[27] Ü. İşci, F. Dumoulin, A.B. Sorokin, V. Ahsen, Turk. J. Chem. 38 (2014) 923-949.

[28] D.V. Tyurin, S.V. Zaitseva, E.V. Kudrik, Russ. J. Phys. Chem. A 92 (2018) 870-875.

[29] O.R. Simonova, S.V. Zaitseva, S.A. Zdanovich, O.I. Koifman, Macroheterocycles 11 (2018) 29-34.

[30] S.V. Zaitseva, E.Yu. Tyulyaeva, O.R. Simonova, S.A. Zdanovich, D.V. Tyurin, O.I. Koifman, J. Coord. Chem. doi: 10.1080/00958972.2018.1506109

[31] A.P. Kroitor, L.P. Cailler, A.G. Martynov, Y.G. Gorbunova, A.Y. Tsivadze, A.B. Sorokin, Dalton Trans. 46 (2017) 15651-15655.

[32] A.B. Sorokin, Bioinorg. React. Mech. 8 (2012) 59-84.

[33] R. Dieing, G. Schmid, E. Witke, C. Feucht, M. Dreßen, J. Pohmer, M. Hanack, Chem. Ber. 128 (1995) 589-598.

[34] C. Ercolani, B. Floris, B. Metal phthalocyanine single-atom bridged dimers. Part 2. Recent results. In *Phthalocyanines: properties and applications;* Leznoff, C. C.; Lever, A. B. P., Eds.VCH: New York, 1996; Vol. 4, pp. 405-425.

[35] V.N. Nemykin, V. Ya. Chernii, S.V. Volkov, N.I. Bundina, O.L. Kaliya, V.D. Li, E.A. Lukyanets, J. Porphyrins Phthalocyanines 3 (1999) 87-98.

[36] F. Monacelli, C. Ercolani, J. Porphyrins Phthalocyanines 5 (2001) 668-673.

[37] N. Mihara, Y. Yamada, H. Takaya, Y. Kitagawa, S. Aoyama, K. Igawa, K. Tomooka, K. Tanaka, Chem. Eur. J. 23 (2017) 7508-7514.

[38] Y. Yamada, M. Okamoto, T. Furukawa, T. Kato, K. Tanaka, Angew. Chem. Int. Ed. 51 (2012) 709-713.

[39] Y. Yamada, N. Mihara, K. Tanaka, Dalton Trans. 42 (2013) 15873-15876.

[40] B. Köksoy, O. Soyer, E.B. Orman, A.R. Özkaya, M. Bulut, Dyes Pigments 118 (2015) 166-175.

[41] W. Zhou, J.R. Thompson, C.C. Leznoff, D.B. Leznoff, Chem. Eur. J. 23 (2017) 2323-2331.

[42] M. Ikeda, H. Murakawa, M. Matsuda, N. Hanasaki, Inorg. Chem. 55 (2016) 7314-7316.

[43] H.Z. Uzunmehmetoğlu, H.Y. Yenilmez, K. Kaya, A. Koca, A. Altindal, Z.A. Bayir, Inorg. Chem. Acta 429 (2017) 51-62.

[44] L.A.Lapkina, Yu.G. Gorbunova, V.E. Larchenko, A.Yu. Tsivadze, Prot. Met. Phys. Chem. Surf. 51 (2015) 204-211.

[45] N. Kobayashi, A.B.P. Lever, A. B. P. J. Am. Chem. Soc. 109 (1987) 7433-7441.

[46] L.A. Lapkina, V.E. Larchenko, G.A. Kirakosyan, A.Yu. Tsivadze, S.I. Troyanov, Yu.G. Gorbunova, Inorg. Chem. 57 (2018) 82-85.

[47] L.A. Lapkina, S.E. Nefedov, Y.G. Gorbunova, A.Y. Tsivadze, Russ. Chem. Bull. 62 (2013) 1930-1933.

[48] K.J. Wynne, Inorg. Chem. 24 (1985) 1339-1343.

[49] M.P. Donzello, M. Fujimori, Y. Miyoshi, H. Yoshikawa, E. Viola, K. Awaga, C. Ercolani, J. Porphyrins Phthalocyanines 14 (2010) 343-348.

[50] S.G. Semenov, M.E. Bedrina, J. Struct. Chem. 58 (2017) 441-446.

[51] K. Oniwa, S. Shimizu, Y. Shiina, T. Fukuda, N. Kobayashi, Chem. Commun. 49 (2013) 8341-8443.

[52] Z. Zhao, A.N. Cammidge, D.L. Hughes, M.J. Cook, Org. Lett. 12 (2010) 5138-5141.

[53] Y. Yang, B. Samas, V.O. Kennedy, D. Macikenas, B.L. Chaloux, J.A. Miller, R.L. Speer, Jr., J. Protasiewicz, A.A. Pinkerton, M.E. Kenney, J. Phys. Chem. A 115 (2011) 12474-12485.

[54] A.N. Cammidge, F. Nekelson, D.L. Hughes, Z.X. Zhao, M.J. Cook, J. Porphyrins Phthalocyanines 14 (2010) 1001-1011.

[55] Z. Zhao, A.N. Cammidge, M.J. Cook, Chem. Commun. (2009) 7530-7532.

[56] Ö. Güngör, M. Durmuş, V. Ahsen, Turk. J. Chem. 41 (2017) 803-812.

[57] T. Guchhait, S. Sasmal, F.S.T. Khan, S.P. Rath, Coord. Chem. Rev. 337 (2017) 112-144.

[58] W. Xu, K. Dziedzic-Kocurek, M. Yu, Z. Wu, A. Marcelli, RSC Adv. 4 (2014) 46399-46406.

[59] Y. Hou, Y. Zhu, J. Sun, X. Zhang, Y. Tian, J. Jiang, CrystEngComm 17 (2015) 4699-4704.

[60] A. Fidalgo-Marijuan, G. Barandika, B. Bazan, M.K. Urtiaga, E.S. Larrea, M. Iglesias, L. Lezama, M.I. Arriortua, Dalton Trans. 44 (2015) 213-222.

[61] A. Aguiar, S. Ribeiro, A.M.N. Silva, L. Cunha-Silva, B. de Castro, A.M.G. Silva, S.S. Balula, Appl. Catal. A : Gen. 478 (2014)267-274.

[62] A.M.N. Silva, A. Aguiar, S.S. Balula, A.M.G. Silva, M. Rangel, J. Mass Spectrom.49 (2014) 763-765.

[63] M. Khorasani-Motlagh, M. Noroozifar, J. Saffari, B.O. Patrick, J. Structr. Chem. 53 (2012) 593-597.

[64] B. Cheng, J.D. Hobbs, P.G. Debrunner, J. Erlebacher, J.A. Shelnutt, W.R. Scheidt, Inorg. Chem. 34 (1995) 102-110.

[65] H.M. Lee, M.M. Olmstead, G.G. Gross, A.L. Balch, Crystal Growth & Design 3 (2003) 691-697.

[66] P.A. Stuzhin, A. Ul-Haq, S.E. Nefedov, R.S. Kumeev, O.I. Koifman, Eur. J. Inorg. Chem. (2011) 2567-2578.

[67] D. Kuter, S.J. Benjamin, T.J. Egan, J. Inorg. Biochem. 133 (2014) 40-49.

[68] D. Kuter, V. Streltsov, N. Davydova, G.A. Venter, K.J. Naidoo, T.J. Egan, J. Inorg. Biochem. 154 (2016) 114-125.

[69] D. Kuter, V. Streltsov, N. Davydova, G.A. Venter, K.J. Naidoo, T.J. Egan, Inorg. Chem. 53 (2014) 10811-10824.

[70] J.M. Gottfried. Surf. Sci. Rep. 70 (2015) 259-379.

[71] M. Li, D. den Boer, P. Iavicoli, J. Adisoejovo, H. Uji-i, M. Van der Auweraer, D.B. Amabilino, J.A.A.W. Elemans, S. De Feyter, J. Am. Chem. Soc. 136 (2014) 17418-17421.

[72] P. Zardi, D. Intrieri, D. M. Carminati, F. Ferretti, P. Macchi, E. Gallo, J. Porphyrins Phthalocyanines 20 (2016) 1156-1165.

[73] Nandi G and Sarkar S. J. Porphyrins Phthalocyanines 18 (2014) 281-289.

[74] N.G. Bichan, E. Tu. Tyulyaeva, I.A. Khodov, T.N. Lomova, J. Mol. Struct. 1061 (2014) 82-89.

[75] M.S. Yusupov, C. Celik, M.R. Geraskina, A. Yoshimura, V.V. Zhdankin, V.N. Nemykin, Tetrahedron Lett. 55 (2014) 5687-5690.

[76] C. Colomban, E.V. Kudrik, D.V. Tyurin, F. Albrieux, S.E. Nefedov, P. Afanasiev, A.B. Sorokin, Dalton Trans. 44 (2015) 2240-2251.

[77] D. Pietrangeli, G. Garramone, M.R. Guascito, A. Pepe, A. Rosa, G. Ricciardi, J. Porphyrins Phthalocyanines 17 (2013) 870-880.

[78] I. Aviv-Harel, Z. Gross, Chem. Eur. J. 15 (2009) 8382-8394.

[79] L. Simkhovich, A. Mahammed, I. Goldberg, Z. Gross, Chem. Eur. J. 7 (2001) 1041-1055.

[80] S.Ganguly, H. Vazquez-Lima, A. Ghosh, Chem. Eur. J. 22 (2016) 10336-10340.

[81] M. Stefanelli, S. Nardis, L. Tortora, F.R. Fronczek, K.M. Smith, S. Licoccia, R. Paolesse, Chem. Commun. 47 (2011) 4255-4257.

[82] J.-I. Setsune, A. Tsukajima, N. Okazaki, J. Porphyrins Phthalocyanines 13 (2009) 256-265.

[83] K. Ueta, M. Fukuda, G. Kim, S. Shimizu, T. Tanaka, D. Kim, A. Osuka, Chem. Eur. J. 24 (2018) 7637-7646.

[84] S. Nardis, F. Mandoj, R. Paolesse, F.R. Fronszek, K.M. Smith, L. Prodi, M. Montalti, G. Battistini, Eur. J. Inorg. Chem. (2007) 2345-2352.

[85] T. Furuyama, Y. Sugiya, N. Kobayashi, Chem. Commun. 50 (2014) 4312-4314.

[86] C.G. Claessens, D. González-Rodriguez, T. Torres, Chem. Rev. 102 (2002) 835-853.

[87] M. Geyer, F. Plenzig, J. Rauschnabel, M. Hanack, B. del Rey, A. Sastre, T. Torres, Synthesis (1996) 1139-1151.

[88] N. Kobayashi, T. Ishizaki, K. Ishii, H. Konami, J. Am. Chem. Soc. 121 (1999) 9096-9110.

[89] J.D. Dang, M.V. Fulford, B.A. Kamino, A.S. Paton, T.P. Bender, Dalton Trans. 44 (2015) 4280-4288.

[90] Y. Yamasaki, T. Mori, Bull. Chem. Soc. Jpn. 84 (2011) 1208-1214.

[91] M.V. Fulford, A.J. Lough, T.P. Bender, Acta Cryst. B68 (2012) 636-645.

[92] Y. Takeuchi, A. Matsuda, N. Kobayashi, J. Am. Chem. Soc. 129 (2007) 8271-8281.

[93] S. Shimizu, A. Matsuda, N. Kobayashi, Inorg. Chem. 48 (2009) 7885-7890.

[94] T. Furuyama, Y. Sugiya, N. Kobayashi, Macroheterocycles 7 (2014) 139-144.

[95] S.K. Ghosh, R. Patra, S.P. Rath, Inorg. Chem. 49 (2010) 3449-3460.

[96] S. Bhowmik, S.K. Ghosh, S. Layek, H.C. Verna, S.P. Rath, Chem. Eur. J. 18 (2012) 13025-13037.

[97] D. Sil, F.S.T. Khan, S.P. Rath, Inorg. Chem. 53 (2014) 11925-11936.

[98] M.A. Sainna, D. Sil, D. Sahoo, B. Martin, S.P. Rath, P. Comba, S.P. de Visser, Inorg. Chem. 54 (2015) 1919-1930.

[99] D. Sil, S.P. Rath, Dalton Trans. 44 (2015) 16195-16211.

[100] D. Sil, S. Bhowmik, F.S.T. Khan, S.P. Rath, Inorg. Chem. 55 (2016) 3239-3251.

[101] D. Sil, F.S.T. Khan, S.P. Rath, Chem. Eur. J. 22 (2016) 14585-14597.

[102] D. Lai, F.S.T. Khan, S.P. Rath, Dalton Trans. 47 (2018) 14388-14401.

[103] J.M. Hodgkiss, C.J. Chang, B.J. Pistorio, D.J. Nocera, Inorg. Chem. 42 (2003) 8270-8277.

[104] J. Rosenthal, B.J. Pistorio, L.L. Chng, D.J. Nocera, J. Org. Chem. 70 (2005) 1885-1888.

[105] J. Rosenthal, T.D. Luckett, J.M. Hodgkiss, D.J. Nocera, J. Am. Chem. Soc. 128 (2006) 6546-6547.

[106] D.N. Harischandra, G. Lowery, R. Zhang, M. Newcomb, Org. Lett. 11 (2009) 2089-2092.

[107] R. Zhang, E. Vanover, T.-H. Chen, H. Thompson, Appl. Catal. A : Gen. 464-465 (2013) 95-100.

[108] I.M. Wasser, H.C. Fry, P.G. Hoertz, G.J. Meyer, K.D. Karlin, Inorg. Chem. 43 (2004) 8272-8281.

[109] K.W. Kwong, C.M. Winchester, R. Zhang, Inorg. Chim. Acta 451 (2016) 202-206.

[110] E. Vanover, Y. Huang, L. Xu, M. Newcomb, R. Zhang, Org. Lett. 12 (2010) 2246-2249.

[111] R. Zhang, E. Vanover, W. Luo, M. Newcomb, Dalton Trans. 43 (2014) 8749-8756.

[112] F. Puls, H.-J. Knölker, Angew. Chem. Int. Ed. 57 (2018) 1222-1226.

[113] J. Rosenthal, J. Bachman, J.L. Dempsey, A.J. Esswein, T.G. Gray, J.M. Hodgkiss, D.R. Manke, T.D. Luckett, B.J. Pistorio, A.S. Veige, D.G. Nocera, Coord. Chem . Rev. 249 (2005) 1316-1326.

[114] P. Afanasiev, E.V. Kudrik, F. Albrieux, V. Briois, O.I. Koifman, A.B. Sorokin, Chem. Commun. 48 (2012) 6088-6090.

[115] I.Y. Skobelev, E.V. Kudrik, O.V. Zalomaeva, F. Albrieux, P. Afanasiev, O.A. Kholdeeva, A.B. Sorokin, Chem. Commun. 49 (2013) 5577-5579.

[116] C. Colomban, E.V. Kudrik, V. Briois, J.C. Shwarbrick, A.B. Sorokin, P. Afanasiev, Inorg. Chem. 53 (2014) 11517-11530.

[117] M.G. Quesne, D. Senthilnathan, D. Singh, D. Kumar, P. Maldivi, A.B. Sorokin, S.P. de Visser, ACS Catal. 6 (2016) 2230-2243.

[118] C. Colomban, E.V. Kudrik, A.B. Sorokin, J. Porphyrins Phthalocyanines 21 (2017) 345-353.

[119] O.V. Zalomaeva, A.B. Sorokin, O.A. Kholdeeva, Green Chem. 12 (2010) 1076-1082.

[120] J. Zhou, F. Wu, Z. Zhu, T. Xu, W. Lu, Chem. Eng. J. 328 (2017) 915-926.

[121] S. Hematian, I. Kentel, T.E. Shubina, M. Dürr, J.J. Liu, M.A. Siegler, I. Ivanovic-Burmazovic, K.D. Karlin, J. Am. Chem. Soc. 137 (2015) 6602-6615.

[122] S. Hematian, I. Garcia-Bosch, K.D. Karlin, Acc. Chem. Res. 48 (2015) 2462-2474.

[123] A.S. Makarova, E.V. Kudrik, S.V. Makarov, O.I. Koifman, J. Porphyrins Phthalocyanines 18 (2014) 604-613.

[124] I.A. Dereven'kov, S.S. Ivanova, E.V. Kudrik, S.V. Makarov, A.S. Makarova, P.A. Stuzhin, J. Serb. Chem. Soc. 78 (2013) 1513-1530.

[125] M.S. Yusubov, V.N. Nemykin, V.V. Zhdankin, Tetrahedron 66 (2010) 5745-5752.

[126] H.M. Neu, V.V. Zhdankin, V.N. Nemykin, Tetrahedron Lett. 51 (2010) 6545-6548.

[127] E. Tabor, J. Poltovicz, K. Pamin, S. Basag, W. Kubiak, Polyhedron 119 (2016) 342-349.

[128] O.V. Zalomaeva, K.A. Kovalenko, Y.A. Chesalov, M.S. Mel'gunov, V.I. Zaikovskii, V.V. Kaichev, A.B. Sorokin, O.A. Kholdeeva, V.P. Fedin, Dalton Trans. 40 (2011)1441-1444.

[129] K.J. Gallagher, M. Espinal-Viguri, M.F. Mahon, R.L. Webster, Adv. Synth. Catal.358 (2016) 2460-2468.

[130] K. Nakano, K. Kobayashi, T. Ohkawara, H. Imoto, K. Nozaki, J. Am. Chem. Soc. 135 (2013) 8456-8459.

[131] M.-E. Ragoussi, T. Torres, Chem. Asian J. 9 (2014) 2676-2707.

[132] M.-E. Ragoussi, M. Ince, T. Torres, Eur. J. Org. Chem. (2013) 6475-6489.

[133] G. de la Torre, G. Bottari, M. Sekita, A. Hausmann, D.M. Guldi, T. Torres, Chem. Soc. Rev. 42 (2013) 8049-8105.

[134] Y. Chen, M. Hanack, Y. Araki, O. Ito, Chem. Soc. Rev. 34 (2005) 517-529.

[135] T.V. Basova, V.G. Kiselev, F. Latteyer, H. Peisert, T. Chassé, Appl. Surf. Sci. 322 (2014) 242-248.

[136] F. Latteyer, H. Peisert, J. Uihlein, T. Basova, P. Nagel, M. Merz, S. Schuppler, T. Chassé, Anal. Bioanal. Chem. 405 (2013) 4895-4904.

[137] T. Basova, A. Berezin, V. Nadolinny, H. Peisert, T. Chassé, H. Banimuslem, A. Hassan, J. Chem. Phys. 139 (2013) 204710.

[138] M. Karasawa, K. Ishii, J. Phys. Chem. C 120 (2016) 21811-21817.

[139] M. Karasawa, K. Ishii, Phys. Chem. Chem. Phys. 20 (2018) 12241-12247.

[140] J.S. Castrucci, R.K. Garner, J.D. Dang, E. Thibau, Z.-H. Lu, T.P. Bender, ACS Appl. Mater. Interfaces 8 (2016) 24712-24721.

[141] L.J. Williams, A.M. Dowgiallo, K.L. Knappenberger, Jr., Phys. Chem. Chem. Phys. 15 (2013), 11840-11845.

[142] C. Preihs, J.F. Arambula, V.M. Lynch, Z.H. Siddik, J.L. Sessler, Chem. Commun. 46 (2010) 7900-792.

[143] Y. Zhang, J.-Y. Wen, X.-I. Wang, M.H.R. Mahmood, Z.-Y. Liu, H. Wang, L.-N. Ji, H.-Y. Liu, Appl. Organometal. Chem. 28 (2014) 559-566.

[144] M. Schappacher, A. Deffieux, Macromolecules 44 (2011) 4503-4510.

[145] M. Schappacher, A. Deffieux, J. Am. Chem. Soc. 133 (2011) 1630-1633.

[146] D.H. Wang, J.N. Pan, H.H. Li, J.J. Liu, Y.B. Wang, L.T. Kang, J.N. Yao, J. Mater. Chem. A 4 (2016) 290-296.

[147] D.V. Konarev, A.V. Kuzmin, M. Ishikawa, Y. Nakano, M.A. Faraonov, S.S. Khasanov, A. Otsuka, H. Yamochi, G. Saito, R.N. Lyubovskaya, Eur. J. Inorg. Chem. (2014) 3863-3870.

[148] S.V. Dudkin, N.E. Erickson, A.V. Vologzhanina, V.V. Novikov, H.M. Rhoda, C.D. Holstrom, Y.V. Zatsikha, M.S. Yusubov, Y.Z. Voloshin, V.N. Nemykin, Inorg. Chem. 55 (2016) 11867-11882.

[149] O. Kataeva, K. Metlushka, K. Ivshin, A. Kiiamov, V. Alfonsov, M. Khrizanforov, Y. Budnikova, O. Sinyashin, Y. Krupskaya, V. Kataev, B. Büchner, M. Knupfer, Eur. J. Inorg. Chem. (2018) 3344-3353.

[150] I. Nigel-Etinger, I. Goldberg, Z. Gross, Inorg. Chem. 52 (2013) 4139-4141.

[151] A.Yu. Tolbin, V.E. Pushkarev, E.V. Shulishov, L.G. Tomilova, J. Porphyrins Phthalocyanines 16 (2012) 341-350.

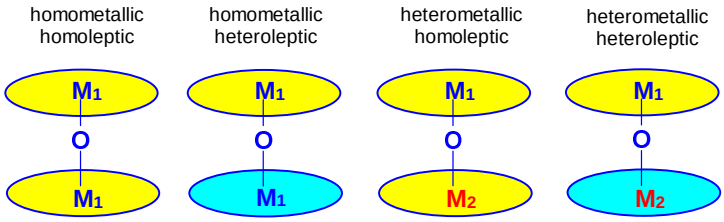

Macrocycles: Porphyrins, Phthalocyanines, Porphyrazines, Corroles, Subphthalocyanine, Subporphyrin

M = Fe, Mn, Ru, Cr, Mo, Re, Al, Si, P, B